Rendered rainscreen walls

Cavity ventilation rates, ventilation drying and moisture-induced cladding deformation

Jörgen Falk

Preface

The work presented in this thesis has been carried out at the Division of Building Materials at Lund University in collaboration with Skanska Sweden. The project has been financed by the Development Fund of the Swedish Construction Industry (SBUF) and Skanska Sweden. Their financial support is gratefully acknowledged.

First of all, I wish to thank my main supervisor Associate Prof. Kenneth Sandin for his skilful help and guidance throughout my work. In addition, I thank my co-supervisor Prof. Manouchehr Hassanzadeh for his help during the last stages of the project. I would also like to express my gratitude to Prof. Lars Wadsö for sharing his valuable knowledge in the art of writing research articles.

I would probably not have started out or completed this project without the enthusiastic support from my industrial supervisor and former manager Sigurd Karlsson. Thanks for your inspiration and commitment!

Thanks also go to the technicians Bengt Nilsson, Stefan Backe and Bo Johansson for all their professional help with the experiments included in the research. Furthermore, I would like to thank all my fellow Ph. D. students at the Division, especially my room companion Henrik Wall.

Last but not least, I would like to thank my girls Annie, Ellie and Lovisa for all their everyday loving support.

Jörgen Falk

Lund, December 2013

Abstract

Over the past five years, moisture damages in external walls of wood frame structure and rendering on insulation as a cladding has been a widely debated subject which has received a lot of attention. In the light of this, the interest in an alternative construction method where rendering is applied on boards instead of insulation has increased. In this method, carrier boards are mounted on battens so that an air cavity is formed between the cladding and the backup wall structure. Provided that this cavity is open at the top and bottom, wind and thermal forces will create air circulation which means that moisture in the wall can be convectively removed.

Under real conditions, ventilation rates in wall cavities are affected by many factors and there is a lack of knowledge regarding both its magnitude and significance for the drying process. Consequently, uncertainties arise during the analysis and moisture safety design of ventilated external walls. The main objective of this study was to increase knowledge of the significance of the cavity design for ventilation rates and convective moisture transport in a cavity behind rendering on a board. Special attention has been paid to the investigation of differences depending on two types of cladding support systems that are often used in practice – vertical wooden battens and perforated horizontal metal battens.

Another objective of the study was to investigate how a cladding made up of rendering and boards is deformed on exposure to moisture changes. Understanding of the deformation behaviour is fundamental in assessing the risk of the occurrence of cracks and other defects that affect the appearance and durability of the rendered façade.

In the theoretical part of the study, applicable equations for the modelling of air flow, heat balance and moisture balance in ventilated cavities were identified. The experimental part comprised an investigation of some important fluid mechanical parameters in a full scale setup in the laboratory, as well as field measurements of air velocity, temperature and relative humidity in experimental walls on a test house in Lund. The walls had four 2.15 m tall and 25 mm deep cavities, and the factor that was varied between the cavities was the design of the cladding support system.

From the field measurements, it was possible to estimate that the average ventilation rate during the period October to February was in the interval 230-310 h^{-1} for the cavity with vertical wooden battens. With perforated metal battens, the ventilation rate was 60-70% lower. Relations between average ventilation rates in the different cavities were roughly in agreement with predictions based on modelled flow characteristics. The study sets out a number of conclusions regarding the way in which wind and thermal forces influenced ventilation rates.

Calculations of average ventilation rates in the cavities of the experimental walls were performed by using tabular climate data for Lund and a simple driving force model. In a comparison of the calculation results and the experimental determination the deviation was less than 20% which indicated that the driving force model was reasonable. With the support of this result, calculations of ventilation rates were made for a number of notional variants of the actual experimental walls, such as different facade colour and different cavity depth.

By applying the knowledge collected, drying rates in ventilated cavities of different designs were calculated during three phases of a drying process. In order to demonstrate the practical significance of the calculation results, drying times for a wet sheathing of gypsum, mounted in the direct vicinity of a cavity, were compared. An example of results from these studies is that the drying time is greatly prolonged if the depth of the cavity is reduced from 10 to 5 mm, but will be only marginally longer if the depth is reduced from 40 to 25 mm.

In practical moisture safety design of ventilated external walls, different types of simulation programs are often used in which the user defines the ventilation rates. The current practice is that the ventilation rate is assumed to have a fixed value, with limited regard to the cavity geometry and the actual climatic conditions. On the basis of the models used in this study, an improved method is suggested for the estimation of realistic ventilation data for use in simulations.

In the deformation study, the material characteristics of rendering and board material which are used in two commercial system solutions were determined. Strips of board material with and without render were then exposed to repeated wetting and drying in an experimental setup, and the free deformations in-plane and out-of-plane were continuously measured. The measurement results were compared with calculations based on a simple mechanical model. Because of limitations in the model and the fact that the influence of gravity had not been eliminated in the experimental setup, measurements and calculations exhibited large differences.

Sammanfattning

Fuktskador i ytterväggar med träregelstomme och putsade isoleringssystem som fasadbeklädnad har de senaste fem åren varit ett mycket uppmärksammat och debatterat ämne i Sverige. Mot denna bakgrund har intresset för en alternativ byggmetod, där puts appliceras på skivor i stället för på isolering, ökat. Metoden innebär att skivor monteras mot läkt så att en luftspalt mellan fasadbeklädnaden och stommen bildas. Förutsatt att spalten är öppen i över- och underkant så kommer vind och termik att skapa en luftomsättning som medger att fukt i väggen konvektivt kan transporteras bort.

Under verkliga förhållanden påverkas luftomsättning i spalter av många faktorer och det finns en kunskapsbrist om både storlek och betydelse för uttorkningsförlopp. Följaktligen uppstår osäkerheter vid analys och fuktsäkerhetsprojektering av ventilerade ytterväggar. Syftet med denna studie har primärt varit att öka kunskapen om spaltutformningens betydelse för luftomsättning och konvektiv fukttransport i en spalt bakom puts på skiva. Speciellt intresse har ägnats åt att undersöka skillnader beroende på två typer av luftspaltsbildande läkt som ofta används i praktiken – vertikala träläkt respektive horisontella, perforerade stålläkt.

Ett ytterligare syfte med studien har varit att undersöka hur en fasadbeklädnad sammansatt av puts och skiva deformeras vid exponering för fuktvariationer. Förståelse för deformationsbeteendet är grundläggande för bedömningar av risk för uppkomst av sprickor och andra defekter som påverkar putsfasadens utseende och beständighet.

I den teoretiska delen av studien identifierades tillämpliga ekvationer för att modellera luftströmning, värmebalans och fuktbalans i ventilerade spalter. Den experimentella delen omfattade undersökning av några viktiga strömningstekniska parametrar i en fullskalig spaltuppställning i laboratorium samt fältmätningar av lufthastighet, temperatur och relativ fuktighet i experimentväggar på ett provhus i Lund. Väggarna hade fyra 2.15 m höga och 25 mm djupa spalter och faktorn som varierades mellan spalterna var läktsystemets utformning.

Från mätningar kunde den genomsnittliga luftomsättningen under perioden oktober till februari uppskattas till intervallet 230-310 h^{-1} för spalten med vertikala träläkt. Med perforerade stålläkt var luftomsättningen 60-70% lägre. Relationer mellan genomsnittlig luftomsättning i de olika spalterna var ungefär i överensstämmelse med prediktion baserad på modellerad flödeskarakteristik. Studien redovisar ett antal slutsatser om hur vind respektive termik influerade luftomsättningen.

Beräkningar av genomsnittlig luftomsättning i experimentväggarnas spalter utfördes genom att använda allmänna klimatdata för Lund och en enkel drivkraftsmodell. Vid jämförelse mellan beräkningsresultaten och den experimentella bestämningen var avvikelsen mindre än 20%, vilket indikerade att drivkraftmodellen var rimlig. Med stöd av detta utfall beräknades luftomsättning för ett antal fiktiva varianter av de faktiska experimentväggarna, till exempel annan fasadkulör och annat spaltdjup.

Genom att tillämpa den samlade kunskapen beräknades fuktutbyte i ventilerade spalter med olika utformning under tre stadier i ett uttorkningsförlopp. För att demonstrera praktisk betydelse av beräkningsresultaten jämfördes uttorkningstider för en blöt vindskyddsskiva av gips monterad i direkt anslutning till en spalt. Ett exempel på resultat från dessa studier är att uttorkningstiden kraftigt förlängs när spaltbredden minskar från 10 till 5 mm men endast blir marginellt längre om spaltbredden minskar från 40 till 25 mm.

Vid praktisk fuktsäkerhetsprojektering av ventilerade ytterväggar används ofta olika typer av simuleringsprogram där användaren definierar luftomsättningen. Rådande praxis är att omsättningen antas till fixa värden med begränsad hänsyn till spaltgeometri och faktiska klimatförhållanden. Baserat på de modeller som används i studien föreslås en förbättrad metod för uppskattning av realistiska luftomsättningar för användning i simuleringar.

I deformationsstudien bestämdes materialegenskaper för puts och skivmaterial som ingår i två kommersiella systemlösningar. Remsor av skivmaterial med och utan puts utsattes därefter för upprepad uppfuktning och uttorkning i en försöksuppställning och de fria axiella deformationerna och böjdeformationerna mättes kontinuerligt. Mätresultaten jämfördes med beräkningar baserade på en enkel mekanisk modell. Beroende på begränsningar i modellen och att inverkan av gravitationen inte eliminerats i försöksuppställningen visade mätningar och beräkningar stora skillnader.

Contents

Appended Papers

This thesis is based on the following papers, which will be referred to in the text by their Roman numerals. The papers are appended at the end of the thesis.

Paper I   Ventilated rainscreen cladding: Measurements of cavity air velocities, estimation of air change rates and evaluation of driving forces

Falk J, Sandin K, (2013)

Building and Environment 59: 164-176

(Published)

Paper II   Ventilated rainscreen cladding: A study of the ventilation drying process

Falk J, Sandin, K, (2013)

Building and Environment 60: 173-184

(Published)

Paper III   Investigation of a simple approach to predict rainscreen wall ventilation rates for hygrothermal simulation purposes

Falk J, Molnár M, Larsson O

(Accepted for publication in *Building and Environment*)

Paper IV   Moisture-induced deformation of multilayer rendered rainscreen structures

Falk J, Molnár M, Hassanzadeh M

(Manuscript)

Contribution of co-authors and other notes

Paper I   KS contributed in the planning and commented on the manuscript. The paper received a 2013 Best Paper Award from journal *Building and Environment.*

Paper II   KS contributed in the planning and commented on the manuscript.

Paper III MM and OL contributed in the planning and commented on the manuscript. MM did the WUFI calulations and wrote the major parts of section 6. Additional solar radiation data were obtained from OL.

Paper IV   MM and MH contributed in the planning and commented on the manuscript. MM did the climatic test cabinet test series measurments.

Notations and definitions

Some of the most used notations in the thesis are listed below.

Notation		Unit
T	Temperature	(°C)
T_{avg}	Average temperature	(°C)
T_c	Cavity air temperature	(°C)
ΔT	Temperature difference	(°C)
p	Air pressure	(Pa)
Δp	Air pressure difference (driving force)	(Pa)
v	Vapour content	$(kg\ m^{-3})$
v_s	Vapour content at saturation	$(kg\ m^{-3})$
Δv	Vapour content difference	$(kg\ m^{-3})$
ρ	Density	$(kg\ m^{-3})$
C_P	Exterior pressure coefficient	
ΔC_P	Exterior pressure difference coefficient	
λ	Friction factor	
ζ	Loss factor	
φ	Relative humidity	
d	Cavity depth	(m)
h	Cavity height	(m)
w	Cavity width	(m)
d_H	Hydraulic diameter	(m)
u_m	Average cavity air velocity	$(m\ s^{-1})$
u_{max}	Maximum cavity air velocity	$(m\ s^{-1})$
G	Convective moisture transport	$(kg\ s^{-1})$

g	Average drying rate	$(kg\ s^{-1}\ m^{-2})$
Z_v	Resistance to vapour flow	$(s\ m^{-1})$
δ_v	Vapour diffusion coefficient	$(m^2\ s^{-1})$
I_{sol}	Solar radiation	$(W\ m^{-2})$
c	Specific heat capacity	$(J\ kg^{-1}\ K^{-1})$

In the thesis, the following terms are synonymous:

(1) <u>screen</u>, <u>rainscreen</u>, <u>cladding</u> and <u>rainscreen cladding</u>

(2) <u>ACH</u> (**A**ir **C**hange rate per **H**our) and <u>ventilation rate</u>

Introduction

Approaches to control rain penetration

The function of building enclosures is to provide a barrier between the indoor and outdoor environment. To meet specific requirements regarding safety, durability and indoor environment quality, a large number of different building techniques and design approaches are available. A major technical factor that always has to be carefully considered in building enclosure design is control of rain penetration.

For exterior walls, the three fundamental system approaches for rain penetration control are storage systems, perfect barrier systems and screened systems [1]. The traditional storage approach utilises the high moisture capacity of massive assemblies made of non-water sensitive materials such as masonry. With the principal function of a water reservoir, these heavy wall systems rely on absorption and storage of rain which penetrates the wall surface until drying to the exterior or interior occurs. In the perfect barrier approach, rain penetration is controlled by a single material layer, assumed to be perfectly watertight. The layer can be arranged at the exterior surface (face sealed) or within the wall assembly (concealed barrier). In the screen approach, the wall is designed with an exterior rainscreen (cladding) that is separated from the backup structure by a continuous air cavity. As the cladding is basically assumed to be an imperfect barrier, the cavity provides drainage to the exterior of water migrating through the cladding. In addition to drainage, cavities may introduce capillary break, ventilation drying and some kind of wind pressure moderation across the screen. In contrast to the compact structure of storage and perfect barrier walls, the two-layer wall design including an air cavity is often referred to as two-stage tightening.

Historically, the incorporation of air cavities in exterior wall systems is not a new invention. For example, the principle has been used in Sweden with wooden claddings since the early 30's according to investigations performed by Lundell [2].

Problem identification

External Thermal Insulation Composite Systems (ETICS) designed to perform as perfect barriers have been used as cladding systems on exterior walls since the 70's in Sweden. In standard installations, insulation is fastened directly to the surface of the backup wall structure and render is applied on top. Originally, the intended use of ETICS was improvement of the thermal performance of existing non-water sensitive

storage walls. However, in the 80's and 90's the application area was expanded to include wood frame backup walls in the construction of new buildings. A typical build-up is schematically shown in Figure 1a. In the 2000's, national investigations led by the SP Technical Research Institute of Sweden found large-scale moisture damage in wood stud/sheathing walls with ETICS assemblies caused by rain intrusion [3]. Because of the numerous damages, a general warning was issued to the Swedish building community about the method. As a consequence, rendered rainscreen walls (Figure 1b) have received increased application in Sweden in recent years.
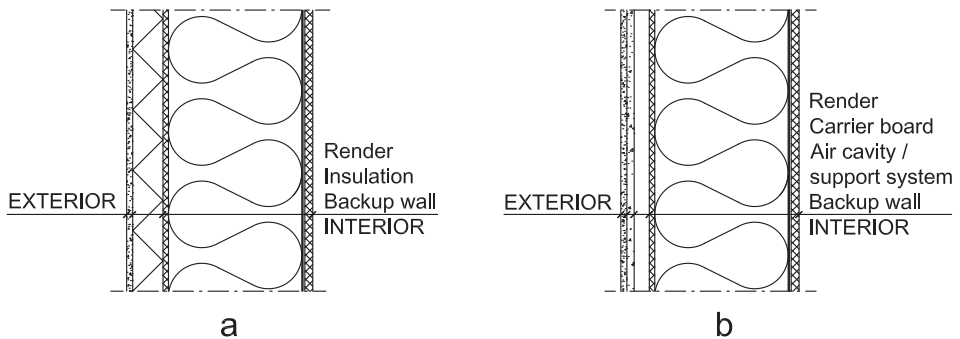

Figure 1.
A compact frame wall with ETICS (a) and a rendered rainscreen wall (b) that provides drainage and cavity ventilation. From the exterior, the two different system approaches appear quite similar.

In Sweden, the failures with ETICS involve considerable economic costs and have caused serious doubts regarding moisture safety and the overall performance of exterior walls with "modern" rendered cladding systems. Notwithstanding the long practical experience of the screen approach, these concerns also include rendered rainscreen walls (Figure 1b). In addition, the national requirements [4] have gradually been clarified and now explicitly demand that moisture safety issues in the building process should be systematically quantified and documented, both in the design and construction phases. For ventilated rainscreen walls, cavity ventilation rate is an important parameter in moisture performance analysis. However, during operating conditions, ventilation rates must vary greatly depending on the cavity design (overall dimension, geometry of cavity openings, configuration of cladding support system etc.) and the outdoor conditions. The many influencing factors mean that ventilation rates in wall cavities are difficult to estimate. From a building physics perspective, there are two crucial consequences of unknown ventilation:

(1) It is difficult to assess and compare the ability of different cavity designs to assist in the drying out process if water has been absorbed by material layers in the wall assembly.

(2) Uncertainty is introduced when simulation programs are used to investigate heat and moisture conditions in ventilated rainscreen walls since this type of tools typically require the user to enter ventilation rates.

In addition to the moisture performance issue, questions arise regarding the mechanical performance of rendered rainscreen assemblies. At early age, initial drying shrinkage occurs and during operating conditions, deformations resulting from changes in cladding temperature and moisture content develop. Due to internal and external restraint to deformations, stresses are induced in the cladding. If cracks develop, the outward appearance and long-term durability of the cladding may be adversely affected. Rendered rainscreen systems are marketed as durable, but information from manufactures regarding properties of individual system components and how the components are designed to mechanically interact is generally moderate. This makes impartial analyzes of the mechanical performance of rendered rainscreen assemblies difficult.

Objectives

The main objective of this thesis was to investigate relationships between cavity design, ventilation rate and ventilation drying for rendered rainscreen walls exposed to north European climate. Differences due to two different cladding support system designs, vertical wooden battens and horizontal vented metal battens, was a priority issue. The results of the doctoral project aim at assisting design engineers to make realistic estimations of cavity ventilation rates and understand the significance of different parameters for the ventilation drying process. An increased knowledge of these two issues improves predictions of how rainscreen walls are influenced by cavity ventilation and respond to different wetting events. A second objective of this thesis was to investigate in-plane and out-of-plane deformations of rendered rainscreen compositions experiencing changes in moisture content. An understanding of the composite deformation behaviour is fundamental to successful analysis of the mechanical performance of full-scale rendered rainscreen assemblies.

Scope and limitations

Quantification of cavity ventilation rates and ventilation drying involves a vast array of parameters and factors. In order to fulfil the main objective of this thesis, the research approach has been broad and focuses primarily on relationships and orders of magnitudes and not precise determinations. The methods used in the thesis include laboratory measurements, full-scale field testing in experimental walls and modelling.

Even if a rendered rainscreen is assumed throughout this thesis, the relevance of the results from the cavity ventilation studies is not limited to this particular cladding type. However, the study exclusively concerns one-storey high walls with an airtight cladding and a backup wall system that only allows for cavity air exchange at horizontal cavity openings spanning the entire cavity width. The latter limitation implies that designs with discontinuous openings, typically used in for example ventilated brick veneer walls, were not dealt with.

In the mechanical part, the scope was limited to laboratory studies of some fundamental material characteristics and free moisture-induced deformations of two commercially available rendered cladding compositions.

Outline of the thesis

The main part of this thesis consists of four appended academic papers. Papers I-II deal with the theoretical and experimental investigations performed regarding cavity ventilation rates and the ventilation drying process. Paper III presents additional data from field measurements and suggests a methodology to model realistic ventilation rate data for hygrothermal simulation purposes. In Paper IV, laboratory measurements of moisture-induced cladding deformations are presented and the results are compared with a simple mechanical model. In the thesis, a summary of each paper is presented in the context in which it is most relevant.

The general context related to this thesis is divided into seven parts. In the first part, a brief overview of ETICS walls and rendered rainscreen walls is provided. In the second part, some relevant theory concerning the building physics of cavity walls is given. The third part describes different methods to estimate cavity ventilation under field conditions and gives an overview of past research findings. Additionally, the third part introduces the field studies of cavity airflow performed in the experimental walls. The fourth part concerns ventilation drying and presents past theoretical and experimental investigations including approaches to model ventilation drying. In the fifth part, drying times following an exterior gypsum sheathing wetting event are calculated and compared for ETICS installations and rainscreen wall assemblies. The

sixth part concerns approaches to predict cavity ventilation rates. The seventh and last part, finally, gives supplementary background information to the deformation behaviour studies and provides findings from field measurements of cladding temperatures and relative humidity boundary conditions in the experimental walls.

Modern rendered cladding systems

The development of exterior insulation systems

In the light of the 1973 oil crisis and the thereby rising energy costs, methods to improve the thermal performance of the existing Swedish building stock became of great interest. At the time, it was estimated that more than one quarter of the total wall enclosure area of houses built before 1960 had external render [5]. Since supplementary thermal insulation is preferably applied on the external wall side, there were demands for methods that preserve the original aesthetics. This motivated Swedish material manufactures to develop and introduce exterior cladding systems where lime-cement render is applied to high-density mineral fibre insulation. In parallel, Swedish researchers investigated the technical performance of such systems [5-9]. Since the cladding systems were primarily intended for thermal improvement of non-water sensitive storage walls, the moisture performance was not considered as a particularly critical issue.

Prior to the Swedish example, exterior insulation systems were developed and used in Germany, France and England [6]. In Germany, lightweight systems with thin synthetic render applied to expanded polystyrene (EPS) were introduced in retrofit applications soon after World War II. In the late 60's, these synthetic and face-sealed perfect barrier systems were introduced and adopted on the North American market. In the nomenclature used today, such synthetic cladding systems are generally referred to as non-drainable EIFS (**E**xterior **I**nsulation and **F**inish **S**ystems) in North America. Unlike the situation in Europe, the North American application area included exterior wood stud/sheathing walls [10]. It should be noted that the term ETICS, preferably used in Europe, relates to systems which use EPS insulation as well as mineral fibre insulation.

In the 80's, the Swedish construction industry began to regularly use mineral fibre insulation and lime-cement render as cladding system in the production of new buildings with wood frame walls. There were several reasons for this progress. The systems offer good thermal performance and they were considered to be both economically advantageous and architecturally attractive. Additionally, the total depth of the compact wall structure is less than for alternatives including an air cavity. In the 90's, EIFS systems were gradually adopted also in Sweden and by the end of the decade, the use of synthetic cladding systems was well established in the Swedish new production of residential buildings as well as other types of buildings.

In North America, serious moisture problems with EIFS used on wood stud/sheathing walls were reported from North Carolina in the mid 90's. In the succeeding years, large-scale failures with EIFS were also reported from several other regions (e.g. Seattle, Vancouver) [11]. The primary cause of the damage was found to be rain intrusion from the exterior through imperfections in the face-sealing around windows and other terminations in the EIFS [10]. Due to the relatively high resistance to vapour flow of the cladding system and the usual presence of a polyethylene vapour barrier close to the interior sheathing, intruding rainwater was trapped in the wall structure and induced mould growth, rot and general material degradation.

In 2007, the SP Technical Research Institute of Sweden issued a general warning to the Swedish building community about the use of ETICS on moisture sensitive substrates [12]. In 2009, the warning was followed up by a comprehensive national report in which experience from surveys of more than 800 buildings was presented [3]. In the report, it was estimated that more than 10 million square metres of ETICS had been installed in the national new production up to 2007, distributed over 15.000-30.000 buildings. Moreover, the survey results indicated that many of these buildings were probably to be damaged by rainwater intrusion in the exterior walls. In an additional report presented by SP 2011 [13], it is stated that the performed surveys showed comparable damage frequencies for mineral fibre and EPS insulation systems.

Rendered rainscreen walls

As a consequence of the failures with ETICS, there are strong incentives in the building industry to use more moisture safe designs of rendered cladding systems, particularly on wood frame structures. Accordingly, efforts have been made to modify ETICS to incorporate some kind of drainage plane in the insulation or between the insulation and the substrate. The principal build-up of another technical approach that is the subject of the present study and that has received increased application in Northern Europe is shown in Figure 2a. Here, the render substrate is not insulation but non-moisture sensitive carrier boards, typically measuring 1200 mm x 800-900 mm x 12 mm. The boards are separated from the backup wall structure by a support system made of wood or metal to create a drained and ventilated air cavity. For fixing the boards to the support system, screws or nails are used. After board installation, render is applied continuously on top and final cladding aesthetic is obtained by an additional finishing layer. Considering the build-up illustrated in Figure 2a, the approach for the rain penetration control is in accordance with the rainscreen principle and gravity driven drainage is expected to remove the majority of water that accidentally penetrates cladding imperfections and joints between the cladding and

windows, doors and other wall components. Furthermore, cavity ventilation driven by wind forces and thermal buoyancy is expected to assist in the removal of water that is absorbed by material layers in the wall structure during operating conditions or during the building process.
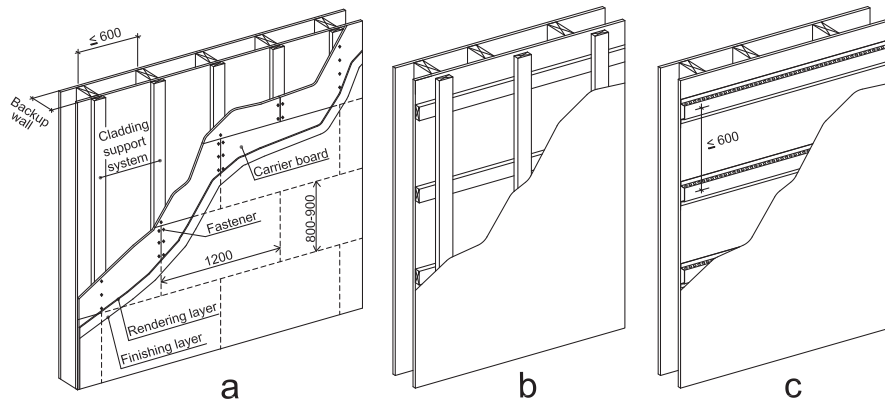

Figure 2.
Illustration of the principal composition of a rendered rainscreen wall (a) and two alternative support system designs (b and c) to create a drained and ventilated cavity between the screen and the backup wall. In configuration c, the horizontal vented supports are made of metal.

Until the mid-2000's, very few buildings in Sweden were designed and built with the rendered rainscreen approach. However, such cladding systems have historically been used in Germany since at least the mid 90's (Figure 3).

Figure 3.
About 1995, this multi-storey building on the outskirts of Berlin was renovated and the exterior walls were supplemented with a rendered and ventilated cladding system.

Considering the design of the cladding support system, each of the three configurations illustrated in Figure 2 has some advantages and disadvantages. The vertical configuration 2a is the most straightforward method to create a ventilated cavity. However, the boards are costly so there are strong incentives to minimize waste of this material by adaptation of the support spacing to the best fit of the size of the boards. This is normally not achievable with configuration 2a as the support placement must be consistent with the placement of the studs in the backup wall. With configuration 2b this particular problem is solved, but a significant disadvantage is an unwanted increase of the total wall depth. For these reasons, configuration 2c with horizontal metal supports has gained increased application in Sweden. To allow for drainage and ventilation despite the horizontal alignment, the webs of the supports are perforated. However, assuming otherwise equal conditions it is obvious that vented metal supports introduce significant resistance to airflow and thus decrease cavity ventilation compared with the unobstructed configuration 2a. Figure 4 shows the use of horizontal metal supports on the ground floor wall of a high-rise building before installation of carrier boards.

Figure 4.
Arrangement of horizontal, vented metal supports with depth 25 mm (left) and a close up which shows the web perforation (right). The function of the green plastic spacers behind the supports is to level out unevenness in the substrate.

In addition to the cladding support system, the design of the cavity openings is an important geometric condition that affects the size of ventilation. In order to direct water that hits wall surfaces, top cavity openings are usually protected with sloped metal flashings whereas bottom openings are often screened by perforated profiles for the purpose of repelling insects and small animals (Figure 5). Usually, the prescribed

design at cavity openings implies that the flow areas are significantly reduced compared with the nominal cavity cross section area.

Figure 5.
Detail showing a bottom cavity opening screened by a vented plastic profile for preventing intrusion of birds, bugs or rodents and for enhancing aesthetics.

Given the previously presented approaches to control rain penetration, it is relevant to comment on a terminology detail concerning screened wall systems. In Pressure Equalized Rainscreen (PER) wall assemblies, the main purpose of the cavity is to instantaneously cancel wind-induced pressure gradient across the cladding and thereby eliminate pressure driven ingress of water to the cavity [14-17]. To achieve pressure equalization, the cavity is not a continuous space but compartmented by horizontal and vertical separators into small volumes, each of which communicates with the outdoor air through strategically placed vent openings through the cladding. For a rapid response time of cavity air pressure, the design of PER walls must carefully consider factors such as ratio of volume to vent area and stiffness and air tightness of the cladding and backup wall, respectively. The pressure equalized wall concept is based on the "open rainscreen principle" which originally was presented in the early 60's [15] and it may be considered as a special type of screened and drained systems [1]. However, since the aim is to equalize pressure, PER walls are not ventilated. Today, terms like "the rainscreen principle" and "rainscreen wall" are commonly associated with a wide range of drained/non-ventilated and drained/back-ventilated wall systems which do not incorporate the essential attributes of PER designs. The capability of such systems to equalize dynamic wind pressures across the cladding is at best moderate [16].

Cavity wall building physics

Driving forces

Airflow in cavities occurs when a driving force is present. For cavity walls, driving force is induced by either wind pressure differences between the cavity openings or by buoyancy, generated by density differences between the cavity air and the outdoor air (Figure 6). If the backup wall is not airtight, air exchange between the cavity and the building interior may also occur (see for example studies made by TenWolde [18] and Bassett et al.[19]). The importance of such unintentional airflow leakage across the wall structure is not considered in the present study.
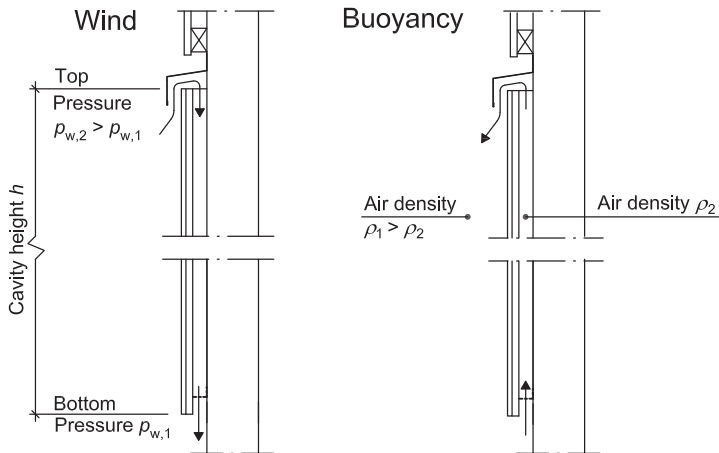
Figure 6.
Illustration of wind-induced and buoyancy-induced airflow in ventilated wall cavities. If the two driving forces act simultaneously, their combined effect determines the total driving force.

When wind hits a building, there is a spatial distribution of wind pressures on the wall surfaces. By means of exterior pressure coefficients C_p (-), the pressure p_w (Pa) at different surface points is described as a fraction of the stagnation pressure at a reference height [20]:

$$p_w = C_p \cdot \frac{\rho_a \cdot U^2}{2} \tag{1}$$

where ρ_a (kg m^{-3}) is the air density and U (m s^{-1}) is the wind speed at the reference height. Exterior pressure coefficients depend on wind direction, building geometry, nearby buildings and obstacles, vegetation and terrain features but not on wind speed [21]. Typically, pressure coefficient distributions for building surfaces are obtained from reduced-scale wind-tunnel tests which allow for systematic variation of different parameters, often with the aim to investigate structural loads. The reference height is then usually equal to the top of the building. Simple static pressure coefficients determined in wind-tunnel experiments on rectangular building shapes are presented in the literature (e.g. [21]). However, for studies of wind-induced cavity airflows, it is the pressure difference Δp_w (Pa) between the top and bottom cavity opening that is of primary interest. The pressure difference is given as:

$$\Delta p_w = \left(C_p^{top} - C_p^{bottom}\right) \cdot \frac{\rho_a \cdot U^2}{2} \tag{2}$$

Due to the stochastic characteristics of the wind, spatial and temporal variations of exterior pressure coefficients are complex. Consequently, results from wind-tunnel model tests give very limited guidance to determine wind-induced driving forces between cavity openings on a wall exposed to real outdoor conditions. Reported field investigations of wind pressure conditions at cavity openings of low-rise walls [22-24] are not conclusive, neither about the size of the pressure difference coefficient ΔC_p nor about the incident wind angles acting for upward and downward cavity airflow, respectively. Attempts to correlate field observations of the direction of cavity airflow with different wind conditions [24, 25] have not been particularly successful.

The density of air decreases as the moisture content and temperature increase. Piñon et al. [26] shows that moisture buoyancy is a significant driving force if the vapour content of the cavity air is considerable higher than the vapour content of the outdoor air. However, in practical contexts such situations are likely to be unusual other than for very short time periods. For this reason, moisture buoyancy effects were excluded from the present study. Thermal buoyancy (also referred to as stack effect) induces a driving force Δp_b which is calculated by the ideal gas law:

$$\Delta p_b = 3462 \cdot \left[\frac{1}{T_a + 273} - \frac{1}{T_c + 273}\right] \cdot h \tag{3}$$

where h (m) is the vertical distance between the cavity openings and T_a (°C) and T_c (°C) is the temperature of the outdoor air and the cavity air, respectively.

If wind and thermal buoyancy are acting simultaneously, the total driving force Δp_{driv} is found as [20]:

$$\Delta p_{driv} = \Delta p_w + \Delta p_b \qquad\qquad (4)$$

While buoyancy only causes vertical pressure gradients, forces from the wind have the potential to create vertical, horizontal and diagonal pressure differences. For cladding support systems consisting of closely spaced vertical wooden battens (Figure 2a), horizontal and diagonal pressure differences are of minor importance. However, if the support system configuration is according to Figure 2b or 2c, there are possibilities for the cavity air to flow in all directions. In an actual rainscreen wall, this may be of significance for cavity ventilation rates. In this study, the issue of horizontal and diagonal airflow was not investigated.

Airflow mechanics

In addition to driving forces, knowledge of cavity airflow versus pressure relationship is fundamental to estimate ventilation rates for wall cavity arrangements. At steady state conditions, forces driving airflow are balanced by pressure drop from friction along the flow path and pressure drops caused by local obstacles, abrupt changes in flow area and sharp bends. In the schematic cavity shown in Figure 6, local pressure drops arise each time airflow passes by or through a horizontal cladding support (see Figure 2b and 2c, respectively) and when airflow enters and exits the cavity.

It is well established from fluid mechanics that airflow in closed conduits of different geometric shapes can be categorised into two distinct flow regimes: laminar and turbulent. In the laminar regime, air flows smoothly and orderly in lamina parallel to the surfaces that define the flow path. In contrast, the turbulent flow regime is characterised by irregularity and mixing of air perpendicular to the flow direction. The laminar velocity profile is parabolic shaped with a large difference between maximum velocity u_{max} (m s^{-1}) and average velocity u_m (m s^{-1}) whereas the turbulent velocity profile has a more flattened out shape (Figure 7). For fully developed laminar flow between two infinite parallel planes, the theoretical ratio of average to maximum velocity u_m/u_{max} (-) is 0.67 [27].

Laminar velocity profile   Turbulent velocity profile

u_{max} u_m Flow u_{max} u_m Flow
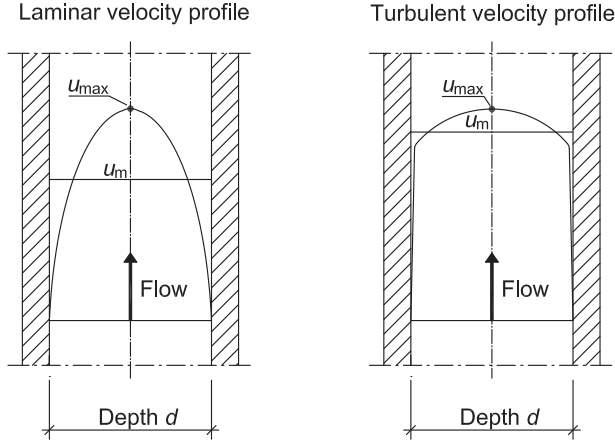
Depth d Depth d

Figure 7.
Illustration of air velocity profiles in the laminar and turbulent flow regime.

The flow regime depends on Reynolds number (Re) defined as [28]:

$$\mathrm{Re} = \frac{u_m \cdot d_H}{\nu}$$
(5)

where d_H (m) is the hydraulic diameter of the cavity and ν (m^2 s^{-1}) is the kinematic viscosity of air. The hydraulic diameter is a geometric parameter and for rectangular shapes, it is a function of the depth-to-width ratio. For shapes where the width w is much larger than the depth d, the hydraulic diameter is close to $2 \cdot d$ (exactly for two infinite parallel planes). Re determines whether the flow is laminar, turbulent or in the transitional zone between these two flow regimes. In pipes and rectangular channels, the flow is laminar if Re is less than about 2000-2300. For fully developed turbulent flow, the Re criteria found in the literature are more unclear and vary between 3500-10000 [21, 29, 30]. Equation (5) implies that the airflow in a wide cavity with depth 25 mm is laminar if the average velocity is less than 0.6-0.7 m s^{-1}. If the cavity depth is only 10 mm, the equation gives that the flow is laminar for air velocities up to about 1.5-1.7 m s^{-1}.

Many studies of cavity wall ventilation have applied equations from the field of fluid mechanics to model airflow in screened wall systems (see for example [22, 24, 26, 29, 31]). In this approach, friction pressure drop is calculated by the well known Darcy-Weisbach friction formula and local pressure drops are handled using the concept of local loss factors. Accordingly, for a cavity with height h (m) exposed to driving force Δp_{driv}, the cavity air pressure balance can be written:

Paper I (pp 166-169)

Laboratory measurements to determine local loss factors and velocity profile ratios

Paper I presents laboratory measurements of loss factors for two types of vented metal battens and various design details at the cavity openings. In the experimental set-up, a cavity lying on the floor was connected to an axial fan with variable rotation speed via a rectangular pressure box. Downstream from the fan, the air was transported in a tube and the volumetric flow rate was determined from the static pressure differential across an orifice plate. For different flow rates, simultaneous pressure drops across local components in the flow path were measured with a differential manometer. Based on the pressure drops and the flow rates, individual loss factors were evaluated as functions of the air velocity. In addition to the pressure measurements, the maximum air velocity at mid-depth in the cavity centre axis was measured with a thermo anemometer with the purpose to investigate the ratio of average to maximum velocity. Without vented metal battens in the cavity, the ratio in the laminar flow regime correlated well with the theoretical ratio 0.67. With vented metal battens, the corresponding ratio was higher, indicating a more flattened out shape of the laminar velocity profile

$$\Delta p_{\text{driv}} = \lambda \cdot \frac{h}{d_{\text{H}}} \cdot \frac{\rho_{\text{a}} \cdot u_{\text{m}}^2}{2} + \sum_{i=1}^{k} \zeta_i \cdot \frac{\rho_{\text{a}} \cdot u_{\text{m},i}^2}{2} \qquad (6)$$

where λ (-) is the friction factor and the second term is the sum of all local pressure losses in the flow path.

For laminar airflow between two infinite parallel planes, the friction factor is 96/Re. For finite rectangular shapes, the factor must be corrected with respect to the aspect ratio d/w. In contrast to the laminar friction factor which only depends on Reynolds number, the transitional and turbulent friction factor are functions of both Re and the ratio ε/d_{H} (-) where ε (m) is the absolute surface roughness. The absolute surface roughness is a measure of irregularities in the surface profile. For example, measurements conducted by Kronwall [29] gave that the surface roughness for gypsum boards and for concrete cast on plywood is in the range of 0.2-0.7 mm and 1.3-2.0 mm, respectively. In the literature, a number of different expressions are available to analytically determine the turbulent and transitional friction factor.

In Equation (6), local pressure drops are described by a specific loss factor ζ_i (-) and the average air velocity $u_{m,i}$ (m s^{-1}). The loss factor can relate to the average air velocity upstream, downstream or within the geometry causing local pressure drop. Figure 8 illustrates cavity airflow that is forced to pass a local obstacle in the flow path. At passage, the airflow contracts and the velocity increases. After passage, the airflow expands and the downstream velocity is regained. The contraction and expansion of the airflow causes a total pressure drop that in Figure 8 is given by a loss factor relating to the air velocity within the obstacle. For clarity, it can be added that the loss factor adopts a lower value if it relates to the velocity before or after the obstacle.
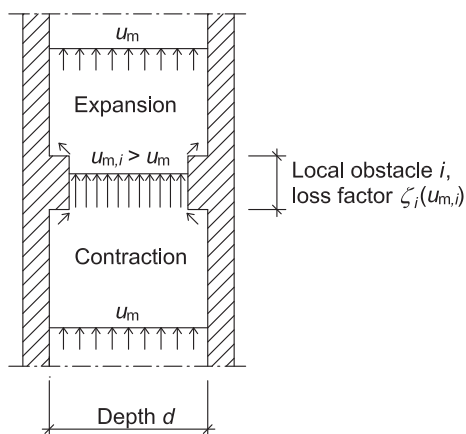

Figure 8.
The figure illustrates a local obstacle in the cavity flow path. When airflow passes, it contracts and expands which give rise to pressure drop. In this example, the size of pressure drop is given by a loss factor relating to the average air velocity within the obstacle.

There are many handbooks and other sources that give loss factors for different geometrical shapes, either as constants or as functions of the velocity. For most cases however, they apply to HVAC (**H**eating, **V**entilation and **A**ir **C**onditioning) system design and assume much higher air velocities than is found in ventilated wall cavities. In addition, the aspect ratio of wall cavities is quite extreme compared with the geometries used in HVAC applications. Consequently, it is difficult to find loss factors that are relevant to estimate pressure drops due to different types of design details used in cavity walls. Measurements of loss factors performed in the present study are presented in *Paper I (pages 166-169)*.

Heat balance

For studies of cavity ventilation rates and ventilation drying, the air temperature profile from cavity bottom to cavity top is of major interest. Firstly, the cavity air temperature is a fundamental input parameter to calculate airflow driven by thermal buoyancy. Secondly, the temperature of the cavity air is needed in studies of the cavity ventilation drying process.

When air flows in cavities, there is a heat exchange between the cavity surfaces and the air. Figure 9 illustrates the longitudinal cavity air temperature profile $T_c(x)$ (°C) behind a cladding exposed to incident solar radiation I_{sol} (W m^{-2}). If the cavity is non-ventilated, the cavity air temperature adopts a uniform equilibrium temperature T_{eq} (°C) determined by the material properties of the wall components and the indoor and outdoor boundary conditions. For the case of ventilation, the temperature of the entering air T_{en} (°C) gradually increases along the flow path. If the air velocity is sufficiently low or the cavity is sufficiently long, the exit temperature T_{ex} (°C) is completely adapted to the equilibrium temperature.

Figure 9.
Illustration of the temperature profile in the cavity air behind a cladding exposed to solar radiation. The figure layout is largely taken from Nevander et al. [32].

At steady-state conditions, the cavity air temperature $T_c(x)$ changes exponentially and is expressed as [20]:

$$T_c(x) = T_{eq} - (T_{eq} - T_{en}) \cdot e^{-x/L_0}$$ (7)

where L_0 (m) is a characteristic length which depends on the specific heat capacity c (J kg^{-1} K^{-1}) and density ρ (kg m^{-3}) of air, the cavity depth d (m), the air velocity u_m (m s^{-1}), the convective heat transfer coefficient α_{cc} (W m^{-2} K^{-1}) at the cavity surfaces, the radiative heat transfer coefficient α_{rc} (W m^{-2} K^{-1}) between the surfaces and the heat resistance of the cladding R_{cl} (m^2 K W^{-1}) and backup wall R_w (m^2 K W^{-1}). To account for exterior surface convection, solar radiation and long-wave sky radiation in calculations with Equation (7), it is convenient to use the equivalent exterior temperature in determining the cavity equilibrium temperature T_{eq}.

As Equation (7) assumes steady-state conditions, the influence of the wall materials' heat capacity is not considered. Under conditions with solar radiation, the heat capacity delays development of cladding equilibrium temperature during heating and prolongs cladding temperature cooling when radiation is reduced or disappears. If the heat capacity is large, the duration of solar radiation may be insufficient to reach steady-state temperature conditions in the wall materials and consequently in the cavity air. For a material layer with infinitely high heat conductivity placed on insulation with which no heat exchange occurs, Claesson et al. [33] give an approximate equation to estimate the impact of heat capacity for the material temperature development at an instantaneous heat supply increase. Material properties considered in the equation are density ρ (kg m^{-3}), specific heat capacity c (J kg^{-1} K^{-1}) and thickness t (m). Figure 10 shows the uniform material temperature T (°C) as a function of these properties and time for a material layer that is initially in equilibrium with temperature 15 °C and is suddenly exposed to heavy solar radiation.
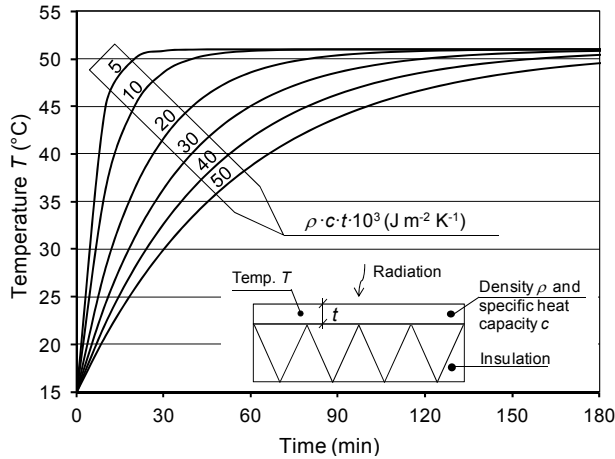
Figure 10.
Temperature development in a material layer placed on insulation as a function of time and the product of density, heat capacity and thickness. Assumptions for the figure results are: initial material temperature 15 °C, surface heat resistance 0.07 m² K W⁻¹, solar radiation 540 W m⁻² and surface solar absorptivity 0.9.

For claddings composed of render applied on boards, the product $\rho \cdot c \cdot t$ is typically in the range $10 \cdot 10^3 – 25 \cdot 10^3$ J m⁻² K⁻¹ and Figure 10 gives that about 90% of the equilibrium temperature is reached within 30–60 minutes. On a real rendered rainscreen wall, the impact of heat capacity on the cavity air temperature can be estimated by studying the results presented in Figure 15. In the figure, the thermal buoyancy driving the daytime ventilation was determined using Equations (3) and (7) and the calculated ventilation rates thus indirectly reflect the temperature in the cavity air behind the rainscreen ($\rho \cdot c \cdot t$ about $25 \cdot 10^3$ J m⁻² K⁻¹). Furthermore, the experimentally determined ventilation rates during daytime hours reflect the true cavity air temperature. Figure 15 clearly indicates a time delay of the true cavity air temperature in the range 1–2 hours which can be attributed to the heat capacity of the wall materials. For the purpose of the present study, the effect of time delay was of little importance and calculations based on Equation (7) were considered sufficiently accurate.

Flow rates

Possible approaches to describe cavity airflow include mass flow (kg s⁻¹ alt. kg s⁻¹ m⁻²), volume flow (m³ s⁻¹ alt. m³ s⁻¹ m⁻²) and **A**ir **C**hange rate per **H**our (h⁻¹), usually abbreviated to ACH. The latter parameter is probably the most recognised amongst

design engineers and it is also well established within the research field. ACH is therefore the parameter that was used in this study and for cavity airflow with constant flow direction, it is calculated as:

$$ACH = \frac{u_{\mathrm{m}}}{h} \cdot 3600 \qquad (8)$$

where u_{m} is the time-averaged cavity air velocity during the time period the ACH calculation refers to. For cavity airflow frequently changing direction, application of Equation (8) may overestimate the ACH.

Convective moisture transport

Convective moisture transport and ventilation drying in cavities occurs when moisture is transferred from adjacent material surfaces to the cavity air so that the vapour content of the exiting air v_{ex} (kg m^{-3}) exceeds the vapour content of the entering air v_{en} (kg m^{-3}). The convective moisture transport rate G (kg s^{-1}) is calculated as:

$$G = (v_{\mathrm{ex}} - v_{\mathrm{en}}) \cdot d \cdot w \cdot u_{\mathrm{m}} \qquad (9)$$

For calculation of the average surface drying rate g (kg s^{-1} m^{-2}), Equation (9) rearranges to:

$$g = (v_{\mathrm{ex}} - v_{\mathrm{en}}) \cdot \frac{d \cdot u_{\mathrm{m}}}{h} \qquad (10)$$

A general restriction for the size of convective moisture transport is that the vapour content of the exiting air is limited by the saturation vapour content, determined by the exiting cavity air temperature.

Wetting mechanisms

On some occasions during construction or service life, it is expected that material layers in wall structures are exposed to high moisture levels. For example, the initial moisture content of autoclaved aerated concrete is generally high on delivery to building sites and therefore requires considerable in service drying to reach equilibrium with the surrounding climate. For other typical wall components such as wood, insulation and sheathing materials, improper material storage procedures on the building site and insufficient rain protection during the assembly process can result in high initial moisture contents.

In wall enclosure service life, there are many moisture sources and transport mechanisms that can induce material wetting. If the wall structure is not airtight, exfiltration of moist indoor air may cause condensation in the exterior parts of the wall assembly. In ventilated cavity walls, it is well known that ventilation not only has the capacity to promote drying but may also lead to cavity condensation due to sky cooling of cladding during clear nights. Under the influence of solar heating, there are possibilities that moisture absorbed by claddings with a high moisture storage capacity (e.g. brick veneer) is redistributed and condenses in the internal and colder wall parts. An important wetting mechanism is wind-driven rain penetration to the cavity space behind the cladding where non-drained water is possibly trapped in depressions and on horizontal surfaces or is absorbed by materials adjacent to the cavity. In extreme cases, wind-driven rainwater may intrude the stud space behind the exterior sheathing of layered frame walls. According to the ASHRAE standard 160P [34], an evenly distributed cladding penetration rate of 1% of the wind-driven rain load should be accounted for as a criterion in the design analysis of above grade building envelopes.

A complicating factor of service life wetting events is that they are unlikely to result in material wetting with a uniform intensity over the entire surface area. This is especially obvious for accidental rainwater penetration at weak points in the cladding assembly (such as cladding terminations at window perimeters) which only causes wetting of portions of the surface. Compared with the case of evenly distributed material wetting, drying analysis of non-uniform wetting events is more difficult to perform and may require two- or three-dimensional approaches for accurate predictions.

Cavity ventilation under field exposure conditions

Measurement techniques

Cavity ventilation rates can be estimated using different measurement techniques. In the constant emission tracer gas method, gas (e.g. N_2O) is injected into the cavity space and the flow rate (or the air velocity) is directly evaluated from the tracer emission rate and the gas concentration in the cavity air and atmosphere. Tracer gas experiments in ventilated wall cavities have been carried out by Sandin [25], Gudum [24] and Basset et al. [19, 35]. The latter two authors remark that the long response time of the method makes it unsuitable for measurements of instantaneous airflows but agree that the method is useful for long-term measurements (days) of average flow rates.

A second approach to estimate cavity airflow rates is to point measure the air velocity with a thermo anemometer. In order to estimate the average air velocity across the cavity depth, the measurement result must be corrected with respect to the shape of the velocity profile (Figure 7). A typical and major concern of thermo anemometers is that they only measure the absolute value of the air velocity while no information is given about the direction of the airflow (upward or downward). If the direction frequently changes, a direct conversion of air velocity to ventilation rate with Equation (8) may introduce significant errors. Another limitation with the anemometer method that is pointed out by Gudum [24] and Saelens et al. [36] is that several individual measuring points may be needed to accurately obtain the horizontally average air velocity across the cavity width. However, in velocity measurements with multiple anemometers in a cavity measuring 1650 mm x 559 mm x 25 mm (*h* x *w* x *d*) performed by Gudum [24], the velocity variation across the width was found to be moderate. An advantage of the anemometer method is that it has short response time and therefore captures cavity velocity changes due to wind fluctuations more effectively than the tracer gas method.

For qualitative studies of airflow in wall cavities, smoke visualization can be used. With the method, it is possible to determine if the flow direction is upward, downward or unstable. It is also possible to make rough estimations of the air velocity, provided it is not too high or low. A significant limitation of the method is that it only gives snapshots of the air exchange process. Thus, smoke visualization is not applicable for assessing ventilation rates in wall cavities over time. In addition, the

method requires a transparent wind barrier and removal of wall insulation in order to study cavity smoke patterns. If there are temperature differences between the indoor air and cavity air, removal of insulation rapidly disturbs the natural cavity conditions.

Previous field measurements

In the past, researchers have made in-situ measurements of air velocities in ventilated wall cavities on many occasions. In a comprehensive literature review of research carried out until the early 2000's, Straube et al. [37] summarise the main findings from such cavity ventilation studies. Because of large differences in cladding and support arrangements, cavity geometries and climatic conditions, the air velocities reported in different studies vary widely and in most cases, the researchers seem to have primarily focused on studies of the relationship between cavity air velocity and wind speed. Although it is not clearly stated, it might be assumed that many early reported cavity air velocity measurements have been made using thermo anemometers.

In Denmark, Gudum [24] measured cavity air velocities in a north-facing wall cavity with height 1.65 m on 16 different occasions during daytime conditions. The cavity was free of obstacles and the openings were continuous with the depth of the cavity (25 mm). Tracer gas technique and thermo anemometers were used simultaneously and the average air velocities u_m (Figure 7) determined from the measurements are shown in Figure 11 [24].
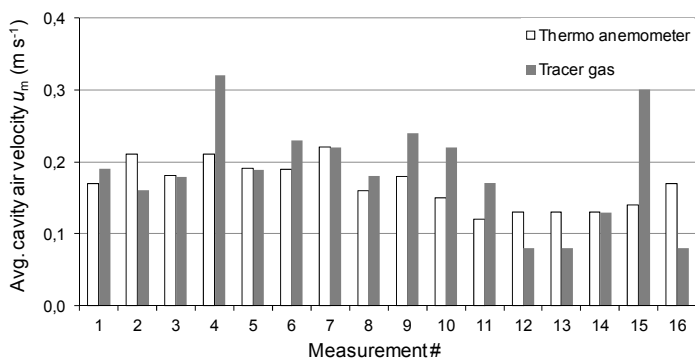

Figure 11.
Measurements performed by Gudum [24]. With the exception of measurement #16 which only lasted for three minutes, the measurement time on each occasion was 5 hours. The average wind speed during the measurements was in the range 0.7–2.1 m s^{-1}.

Figure 11 shows that Gudum [24] determined the average air velocity to be 0.12–0.22 m s^{-1} with thermo anemometers. Using Equation (8) and cavity height 1.65 m, these velocities give ventilation rates of 260–480 h^{-1}. With tracer gas, the corresponding velocities were 0.08–0.32 m s^{-1} (175–700 h^{-1}). The large deviation between the two methods for measurement period #16 was considered to be due to unstable flow direction since such conditions are detected with tracer gas but not with thermal anemometers. No explanation of the poor agreement for measurement period #4 and #15 was found.

In tracer gas field experiments conducted in cavity walls in New Zealand, Bassett et al. [19] measured cavity flow rates behind fibre cement board and brick veneer claddings. The height of the cavities was 2.4 m whereas the depth varied: 20 mm behind fibre cement cladding and 40 mm behind brick veneer. Both cladding types were configured with discrete top and bottom vents of nominal area 1000 mm^2 m^{-1}. The measured daily average ventilation rates were in the range 0.5–2.5 L s^{-1} m^{-1} (20–95 h^{-1} for cavity depth 40 mm) with extremes up to 5 L s^{-1} m^{-1}.

In field investigations of brick veneer walls including measurements with thermo anemometer, VanStraaten et al. [38] estimated the ventilation rate to be 0–90 h^{-1} in a cavity measuring 2440 mm x 1220 mm x 20 mm (h x w x d). The venting configuration consisted of two pairs of clear and open ventilation slots. The size of each slot was approximately 10 mm x 80 mm, giving a nominal vent area of 1300 mm^2 m^{-1} at the top and bottom.

Sandin [25] carried out tracer gas measurements in brick veneer cavity walls with height and depth about 2.5 m and 20 mm, respectively. The cavities were configured with continuous top openings and discrete bottom ventilation slots at typical spacing (vent area of about 1000 mm^2 m^{-1}). The measured ventilation rate was below 10 h^{-1}. In addition to tracer gas, Sandin [25] used smoke injections for detail studies of cavity airflow patterns behind the brick veneer. The smoke tests showed that the airflow was very unstable.

Some past research studies emphasise that mortar protrusions and mortar droppings may significantly reduce airflow in wall cavities behind brick veneer (e.g. [38]). However, no discussions and experimental investigations concerning the reducing impact of horizontally aligned perforated cladding support systems on cavity airflow have been found in the literature.

Experimental set-up and airflow studies

In the present study, south-facing experimental walls including 4 cavities were built in a test house (Figure 12). The test house is located in Lund, in the southern most part of Sweden.
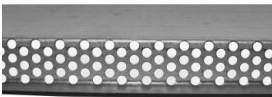

Figure 12.
Exterior and interior view of the south-facing experimental walls (the walls are marked with a white dashed line in the exterior view). In the interior view, the 145 mm mineral wool insulation between the studs is removed and the four cavities measuring 2150 mm x 390 mm x 25 mm (*h* x *w* x *d*) are visible through the transparent sheathing (wind barrier) made of Polycarbonate. In each cavity, three temperature sensors and three relative humidity sensors were installed at mid-depth at three points: close to the top and bottom opening and at mid-height. On the roof of the test house, a local weather station registered wind speed, wind direction, outdoor temperature and relative humidity every 10 minutes. Note that both pictures are reproduced in larger size on the back cover of this thesis.

The only difference between the cavities in the experimental walls was the cladding support system and the main purpose of the experimental set-up was to compare cavity ventilation rates for the different configurations during exposure to equal boundary conditions. To prevent airflow between the cavities and the indoor environment (and between the cavities), all material joints were carefully sealed. In cavity 1, the cladding support system was vertical wooden battens whereas cavity 2–4 included four horizontally aligned vented metal battens, spaced 600 mm apart (Figure 12). The perforation patterns for the different metal battens are shown in Table 1.

Table 1.
The vented metal battens types (height 25 mm) that were used in the experimental walls.

Cavity	Perforation	Lateral view	Perspective view
2	Holes φ8 spaced 100 mm in one row. Flow area 503 mm^2 m^{-1}		
3	Holes φ18 spaced 36 mm in one row. Flow area 7069 mm^2 m^{-1}		
4	Holes φ5 spaced 13 mm in six rows. Flow area 9062 mm^2 m^{-1}		

Smoke visualisation tests

Smoke visualization of cavity airflow in the experimental walls was performed with Dräger Airflow Tester. To enable the tests, the insulation between the studs was removed and smoke was injected into the cavities through drilled holes at different positions in the wind barrier. In cavity 2 with minimal ventilation, the air movements were very small and it was not possible to determine the flow direction or estimate the air velocity. In the other three cavities, tests were made on a number of occasions with different wind and cavity air temperature conditions. The complete results from the smoke experiments are reported in Falk [39] and they are not repeated here. Nevertheless, with the method it was difficult to detect any significant differences in air velocity when smoke was injected at mid-depth or closer to the cavity surfaces. This observation was made independent of the batten configuration and indicated a rather flat shape of the velocity profile, even for Reynolds numbers well below 2000. It must however be stressed that the method lacks much of the sophistication required for such detailed studies. The overall most important observation from the smoke tests was that when wind forces acted in absence of significant buoyancy forces, the cavity airflow was often unstable with no clear dominant flow direction.

Paper I (pp 169-176)

Measurements of air velocities in the experimental wall cavities

Paper I presents results from thermo anemometer measurements of air velocities in cavity 1, 3 and 4 on 36 different occasions, distributed from October to February. For the 5 month period, relationships between the time-averaged air velocities in the three cavities approximately agreed with predictions based on modelled flow characteristics of the experimental walls. The forces driving cavity airflow were found to be small, in the order of 0.2-0.3 Pa for significant parts of the measurement time. To enable studies of wind effects, occasions with strong buoyancy and constant upward flow direction were used to evaluate wind-induced airflow in the cavities. It was found that wind-induced pressures frequently changed the cavity airflow direction which in turn significantly reduced the efficiency of the wind to create air exchange. A pressure difference coefficient ΔC_p (-) in the interval 0.025–0.05 was found applicable to estimate solely wind-driven ventilation rates, independent of the angle between the wind and the wall surface.

Thermo anemometer measurements

To estimate long-term ventilation rates in the experimental walls, measurements of cavity air velocities u_{max} (Figure 7) at mid-depth were carried out using a single thermo anemometer. According to the manufacturer specifications, the accuracy of the anemometer is $\pm(0.03$ m s^{-1} + 5% of mean value). Due to the findings in the smoke tests, cavity 2 was excluded from the anemometer velocity measurements. Results from the measurements are presented in *Paper I*.

To verify that Equation (6) provided satisfactory predictions of velocity versus pressure relationships in the experimental wall cavities, air velocity calculations were compared with measurement results obtained on some occasions with dominating thermal driving forces. Two such occasions are shown in Figure 13. The calculation results presented in the figure are based on Equation (6) with application of the laboratory results regarding local loss factors and ratio of average to maximum air velocity u_m/u_{max} (-) (*Paper I*). It should be noted that the calculated air velocities in Figure 13 exclude the influence of wind forces and only consider the thermal driving force Δp_b (Pa), determined from the measured cavity air and outdoor temperatures. As shown by Figure 13, the correlation between the averaged measurement result and the calculations is very good in cavity 4 while there is a systematic deviation about 10% in

cavity 1. From the figure, it is however clear that the wind speed conditions and the temperature differences ΔT (°C) were more favourable for stable buoyancy driven air velocities during the period in cavity 4. Furthermore, the flow characteristics of the two cavities are quite different (*Paper I*) and for cavity 4, designed with vented horizontal battens, the air velocity is only marginally affected by moderate wind-induced pressures if strong buoyancy is established. This characteristic is much less pronounced for cavity 1 with vertical battens and at equivalent buoyancy pressures, wind-induced pressures cause comparatively large velocity variations. Thus, the deviations in cavity 1 may be attributed to wind effects. Considering the average wind angle of 315° (definition is given in Figure 13) and exterior pressure coefficient distributions on wall surfaces of low-rise buildings presented in reference [21], it is expected that wind forces counteracted the upward buoyancy driven airflow during major parts of the time.

In conclusion, Equation (6) and the laboratory determined loss factors and velocity ratios (*Paper I*) were considered reliable for analysis of air velocity data collected during the measurements in the experimental walls.
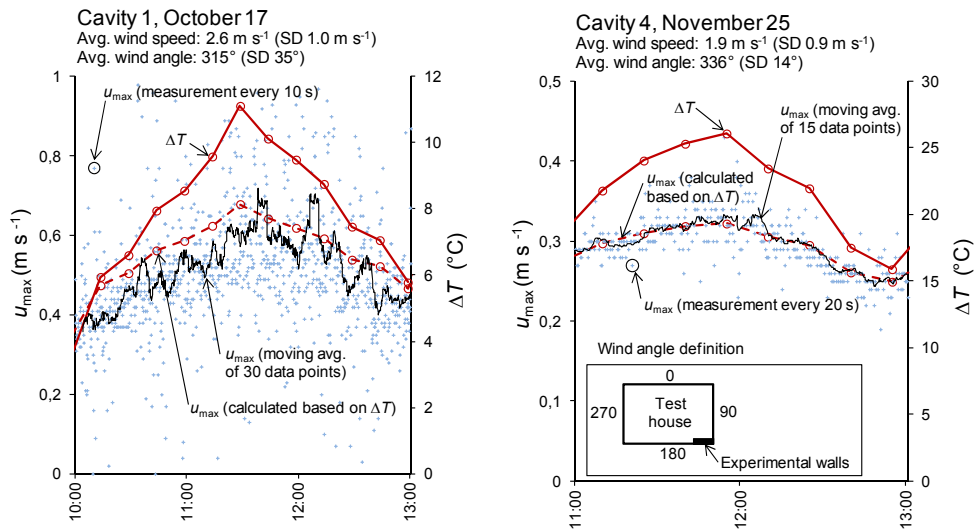

Figure 13.
Comparison between thermo anemometer velocity measurements and velocity calculations based on Equation (6) and the buoyancy force induced by the temperature difference ΔT between the cavity air and outdoor air. Wind angle definition is given in the right diagram.

Ventilation drying

Literature review

A considerable amount of research has been made to investigate moisture conditions in cavity walls and the mechanisms of ventilation drying. With some exceptions, the research has focused on one-storey high wood frame wall assemblies exposed to cool and mixed humid climates found in the Northern Hemisphere.

Theoretical analyses [22, 26, 40, 41] and results from computer simulations [42, 43] tend to show that cavity ventilation effectively benefits drying. Based on the assumptions of airflow rates in the interval 0.05–0.5 L s^{-1} m^{-2} and saturated cavity surfaces, Burnett et al. [22] estimated that the potential cavity ventilation drying rates in a Canadian climate (Waterloo, Ontario) range from 10 to 1000 g day^{-1} m^{-2} . They also conclude that drying rates are about ten times greater in July compared with January. In consideration of many relevant parameters, a theoretical study performed at the Canada Mortgage and Housing Corporation (CMHC) [40] found that the cavity depth is the single most important factor to promote ventilation drying and that potential drying rates significantly decrease if the cavity depth is less than about 12 mm. Assuming wet conditions in a plywood sheathing which face a cavity with height 2.4 m and depth 19 mm, Ge et al. [41] presents ventilation drying rate calculations for different scenarios. For the case the sheathing is assumed covered with a membrane ($Z_v \approx 2.6 \cdot 10^3$ s m^{-1}), they found that drying rates are controlled by the properties of the membrane and not the airflow rate. Without membrane, the maximum calculated drying capacity occurred at cavity air velocity 0.2 m s^{-1}. For higher air velocities, the calculations showed that the exiting air is not saturated and they therefore conclude that an optimum ventilation rate exists. It should be added that the study done by Ge et al. [41] did not consider the effect of solar heating.

Laboratory studies of ventilation drying have been carried out as climate chamber tests [44-47] or as experiments with the main purpose to demonstrate the relationship between ventilation rate and drying rate [48, 49]. While the majority of the reported laboratory research results support the idea that ventilation is beneficial to remove moisture within cavity wall assemblies, there are contradictory findings. In climate chamber tests performed by Lawton et al. [46], water was injected into the stud space of wood frame cavity walls with plywood sheathing and stucco cladding. The drying process was monitored for 150 days under exposure to simulated outdoor climate excluding wind pressures and solar radiation. They conclude that if water enters the stud space of cavity walls, the rainscreen design does not improve the drying potential compared with non-ventilated wall assemblies.

Several full-scale field investigations have been performed to study the influence of cavity ventilation on moisture conditions in wood frame wall assemblies exposed to natural moisture loads. TenWolde et al. [18] monitored moisture conditions in walls which were not airtight. Since moisture conditions in the walls related to indoor relative humidity, they argue that cavity ventilation does not provide reliable drying if air leakage between the interior and the cavity is allowed. For airtight wall assemblies, it was found that cavity ventilation promoted drying. Hansen et al. [50] measured moisture content in wooden components behind and in front of the exterior sheathing in 12 different wall assemblies including both ventilated and non-ventilated cavities. No significant difference in moisture content depending on the ventilation strategy was found. In a study on the influence of a 23 mm deep cavity on moisture content in wooden cladding, measurements conducted by Nore et al. [51] showed that closed cavity openings are beneficial in dry climate situations whereas a design with free openings reduces the cladding moisture content if it is exposed to heavy wind-driven rain.

In a field study from The Fraunhofer Institut für Bauphysik, Popp et al. [52] conducted a 2 year follow up of the decrease in moisture content of backup walls made of initially wet aerated concrete. In the experimental set-up, the walls were designed with an impermeable cladding arranged to allow for ventilation or fixed directly to the concrete. With ventilation, drying of the aerated concrete was found significantly enhanced compared with the non-ventilated case.

In a recent field study carried out by Sandin [53] 2012, the influence of ventilated and non-ventilated external supplementary insulation systems on the drying out time of wet aerated concrete walls was measured and compared. The walls were oriented towards the south and inward drying was limited by a paint layer ($Z_v \approx 18 \cdot 10^3$ s m^{-1}). Before application of the supplementary systems, 20 mm lime-cement render was applied to the outward concrete surfaces. The non-ventilated systems were 3–4 mm synthetic render applied to 50 mm EPS and 20 mm lime-cement render applied to 50 mm mineral fibre insulation, respectively. The ventilated system consisted of 45 mm mineral fibre insulation, wind barrier membrane ($Z_v \approx 2.4 \cdot 10^3$ s m^{-1}), 22 mm vertical cladding support system and 12 mm carrier board including 6–7 mm lime-cement render. For the wall with the synthetic cladding system, findings estimated that the drying out time was 5-6 years. For the other two cases, the wall drying out time was equal and considerably shorter, about 3 years. Thus, the rainscreen approach was not found to improve the wall drying compared with the non-ventilated mineral system.

Field investigations of ventilation drying [54-56] which in addition to natural field exposure conditions include artificial wetting have only been performed to a limited extent. In a comprehensive study presented by Straube et al. [54], five different wood frame cavity walls including integrated wetting systems were monitored for over a year. The wall cladding systems included brick veneer and vinyl siding, both with

back-ventilated cavities of various depths. In one brick veneer wall configuration there were weep holes but no top openings and the cavity was considered non-ventilated. In all walls, a vapour barrier was installed close to the interior wall surface in order to prevent inward drying and the exterior sheathing consisted of high permeance fibreboard covered with membrane of either spun bonded polyolefin or asphalt impregnated felt paper. During the study period, the exterior sheathing was wetted uniformly on the inside facing surface on several occasions. Some of the findings from the study were as follows:

- All wall systems allowed very significant drying but drying rates varied during different weather conditions and they were strongly enhanced during hot and dry outdoor conditions.

- During cold and cool conditions, vinyl siding cladding walls dried significantly faster than brick veneer walls. During hot and dry conditions, drying rates for the two cladding types were similar.

- Brick veneer walls dried more slowly if they not were ventilated. In addition, moisture conditions in the stud space of non-ventilated walls were more unfavourable and they suffered from more condensation wetting caused by solar-driven inward vapour diffusion.

- Sheathing membrane properties influence drying rates and if the vapour permeance is low, ventilation may not benefit the drying process.

In another field investigation including controlled artificial wetting, Drumheller et al. [55] studied the moisture performance of nine different wood frame wall assemblies which were replicated for both south-facing and north-facing exposure. The walls had exterior plywood or oriented strand board sheathing covered with one or two layers of sheathing membranes. On the interior wall surface, two coats of latex paint were applied (possibly to reduce the effect of inward drying). Exterior cladding systems included vinyl and fibre cement siding, stucco, brick veneer and synthetic stone. In some assemblies there was a cavity between the cladding and sheathing. In the wetting procedure, water was injected on both sides of the sheathing membrane and also in between if two membranes were present. For evaluation of performance, the moisture content of the sheathing was monitored. A selection of conclusions that were drawn based on the experiments are summarised below:

Paper II

Calculations of ventilation rates and modelling of the ventilation drying process

Paper II presents calculations of average ventilation rates in the experimental wall cavities for a 5 month period (October to February) and investigates how the ventilation rates are affected by changes in the cavity design and season. The calculations use a simple driving force model and monthly and annual tabular climate data for southern Sweden. For the actual design of the experimental walls, the calculated average ventilation rates and the field measurement findings reported in *Paper I* compared well. Based on the ventilation rate calculations and in consideration of the cavity air temperature profile, a set of basic building physics equations were applied to estimate drying rates in the experimental wall cavities during different stages in the ventilation drying process. The performed calculations show that the cavity design is of major importance for the drying rate if the material adjacent to the cavity is wet over its entire extent. As the drying process proceeds and becomes dependent on diffusion, the drying rates for different cavity designs tend to be evened out. The significance of the derived ventilation drying rates is demonstrated in calculations of drying times for initially wet exterior gypsum sheathing in a layered frame wall.

- Orientation and solar exposure are important factors for wall moisture performance. Generally, north facing walls experienced higher moisture conditions compared with corresponding south-facing walls.

- Brick veneer walls were among the driest walls in the study. 25 mm (1 inch) air cavity along with dark brick colour (high absorptivity for solar radiation) provided increased drying capability.

- In wall assemblies with air cavity, there was no sustained increase in sheathing moisture content during moisture injections.

- Air circulation and high cavity temperature were the two primary mechanisms that acted to lower sheathing moisture content.

The literature review shows that many efforts have been made over the past 10–15 years to study ventilation drying, particularly in North America. Because of differences in building styles, some of the investigated cladding and wind barrier configurations are seldom used in Sweden. Notwithstanding this, the research results

provide insight into the current state of the art and they clearly demonstrate the variety of parameters and mechanisms affecting cavity wall moisture performance.

It may be concluded that the different approaches of previous research tend to show that cavity ventilation has the potential to assist in the drying process of cavity walls, but research results also highlight that ventilation drying is greatly influenced by the:

- exterior climate conditions

- size and physical position of moisture concentrations

- geometry of cavity flow paths

- moisture mechanical properties of individual material layers

However, the literature review also indicates that little attention has been given to model and describe the ventilation drying process in consideration of the size and physical cause of cavity airflow during real operating conditions. In the present study, an investigation of the ventilation drying process and its practical implications during real operating conditions are presented in *Paper II*.

Approaches to model ventilation drying

For estimation of ventilation drying rates, different modelling techniques have been proposed. In a method described by Burnett et al. [22], an equivalent vapour permeance M_{eq} (m s^{-1}) for wall claddings including the effect of ventilation is calculated as:

$$M_{eq} = \frac{1}{Z_{v,clad}} + Q \tag{11}$$

where $Z_{v,clad}$ (s m^{-1}) is the cladding resistance to vapour flow and Q (m^3 m^{-2} s^{-1}) is the airflow rate. If these two parameters and the vapour content v (kg m^{-3}) of the exterior air and cavity air are known, the combined diffusion and convective moisture transport g (kg s^{-1} m^{-2}) can be calculated as:

$$g = M_{eq} \cdot \Delta v \tag{12}$$

where Δv (kg m^{-3}) is the vapour content difference between the cavity air and exterior air. The practical use of Equation (12) is limited to comparing the drying potential of different cladding configurations under conditions of saturated cavity air since the equation assumes ventilation drying rates controlled by the airflow rate.

In a sophisticated approach, Davidovic et al. [48] derived an analytical expression to estimate convective moisture transport G (kg s^{-1}) in ventilated wall cavities where one cavity surface is wet:

$$G = Q \cdot \rho_a \cdot \left[0.62 \cdot \frac{K \cdot p_{v,s}(T_w) + \Phi \cdot \left(p_{v,in} - K \cdot p_{v,s}(T_w)\right)}{p_{atm} - K \cdot p_{v,s}(T_w) - \Phi \cdot \left(p_{v,in} - K \cdot P_{v,s}(T_w)\right)} - W_{in} \right] \qquad (13)$$

where Q (m^3 s^{-1}) is the airflow rate, ρ_a (kg m^{-3}) is the air density, p_{atm} (Pa) is the atmospheric pressure, $p_{v,s}(T_w)$ (Pa) is the partial water vapour pressure of saturation based on the temperature of the wet cavity surface, $p_{v,in}$ (Pa) and W_{in} (-) are the partial water vapour pressure and humidity ratio of the entering air, respectively. In Equation (13), the coefficient K (-) takes into account the effective wetting area of the cavity surface. For the case that the cavity surface is completely saturated, K is equal to 1. The coefficient Φ (-) is a parametric correction function depending on cavity geometry, airflow rate and the thermo physical properties of air. Due to the complexity of the correction function Φ, Equation (13) is difficult to use.

Ventilated rainscreen versus ETICS - relative drying times

In the present study, ventilation drying rates were calculated for the experimental rainscreen walls. Furthermore, the significance of the drying rates was demonstrated in a case study of drying times for gypsum sheathing, initially wet over its entire extent and located on the exterior side of a layered frame construction (*Paper II*). For comparison, it is interesting to estimate gypsum sheathing drying times for cladding installations with non-ventilated ETICS (Figure 14). As for the rainscreen wall calculations, inward drying is assumed prevented and the outward removal of moisture is modelled to occur from the sheathing centre. Furthermore, assumptions of boundary conditions, initial sheathing moisture content and physical and moisture mechanical sheathing properties are identical to the ventilated case. It should be noted that under real conditions, the sheathing dries both inwards and outwards. However, provided there is a vapour barrier close to the interior sheathing of the frame construction, moisture will not dry out inwards from the wall. Thus, the calculations overestimate the time required for the moisture to dry out from the sheathing and

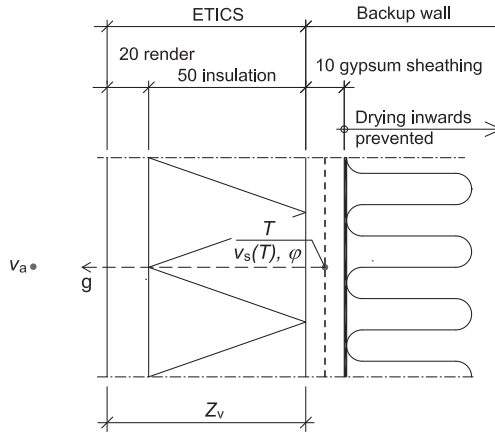underestimate the time required for the moisture to dry out from the wall construction.

Figure 14.
Outward drying from wet gypsum sheathing in an ETICS wall assembly.

With ETICS, drying is controlled by diffusion and the drying rate g (kg s^{-1} m^{-2}) is given as:

$$g = \frac{v_s(T) \cdot \varphi - v_a}{Z_v} \tag{14}$$

where $v_s(T)$ (kg m^{-3}) is the vapour content at saturation for sheathing temperature T (°C), φ (-) is the relative humidity in the sheathing, v_a (kg m^{-3}) is the vapour content of the outdoor air and Z_v (s m^{-1}) is the resistance to vapour flow in the cladding assembly. Using the moisture transport data presented in Table 2, rough estimations of the lower and upper limit of Z_v for ETICS become $15 \cdot 10^3$ and $75 \cdot 10^3$ s m^{-1}, respectively. The lower value applies to systems where render is applied to mineral fibre insulation and assumes a typical insulation density of approximately 100 kg m^{-3}.

Table 2.

Vapour diffusion coefficients δ_v for lime-cement render and insulation (Hedenblad [57]).

Material	Relative humidity (%)	δ_v (10^{-6} m^2 s^{-1})
Lime-cement render	90-95	~ 1.5
	35-90	~1
EPS-insulation, ρ ~20 kg m^{-3}	35-100	0.9–1.3
Mineral fibre insulation, ρ ~15 kg m^{-3}	-	15–24
Mineral fibre insulation, ρ ~200 kg m^{-3}	-	8–12

In Table 3, relative gypsum sheathing drying times for rainscreen walls and ETICS are compared. Geometry and configuration of the ventilated cavity are assumed to comply with wall cavity 1 (Figure 12).

Table 3.

Relative drying times for gypsum sheathing that is initially wet over its entire extent and dries to equilibrium with 80% relative humidity. The rainscreen wall cavity is assumed to comply with cavity 1, shown in Figure 12.

Cladding colour / Direction / Time of year	Rainscreen wall cavity 1	ETICS $Z_v = 15 \cdot 10^3$ s m^{-1}	ETICS $Z_v = 75 \cdot 10^3$ s m^{-1}
Light / South / October–February	1	4	20
Dark / South / October–February	1	6	30
Dark / South / April-August	1	15	75

The results in Table 3 show that for extreme situations with initially wet conditions over the entire gypsum sheathing extent, sheathing drying time with ETICS is in the range 4–75 times longer depending on the cladding colour and time of year. If the rainscreen wall is assumed designed with horizontal cladding supports (according to cavity 3 or 4 in Figure 12) in the comparison, the extended ETICS drying time reduces to a factor 3–40. It should be noted that convective moisture transport in narrow cavities with depth $d < 10$ mm is much less efficient than in cavities with a depth of 25 mm (*Paper II*). For narrow depths, the sheathing drying time in the rainscreen wall assembly might be comparable to the drying time with non-ventilated ETICS [39].

Ventilation rate predictions

In building enclosure design, engineers often use hygrothermal simulation programs for verifying moisture performance of wall and roof assemblies. Along with the ever expanding possibilities that this type of programs offer, the need for detailed and reliable input data regarding material properties and different variables increases. For simulations of ventilated rainscreen walls, it is typically expected that the user provides ventilation rate data and if such data is not based on physical grounds, it can impair the quality of the simulation results [58, 59].

Predictions of cavity ventilation rates basically require knowledge of:

(1) relationships between pressure and airflow rate for cavity flow paths

(2) forces available for driving airflow

While modelling of cavity airflow characteristics is fairly well described in the literature, procedures that can be used to model wind and buoyancy forces driving cavity ventilation under field exposure conditions are less well developed and with a few exceptions, the issue is rarely discussed in the literature.

In one deliverable report from a comprehensive R&D project funded by ASHRAE, Piñon et al. [26] propose a methodology for estimating cavity ventilation potentials for different types of cladding systems. In the recommended procedure, average wind forces driving cavity ventilation are calculated based on annual average wind speeds and a zonal model of wall pressure coefficient distributions, relying on general data from wind tunnel experiments and findings from field tests performed by Straube et al. [22]. Furthermore, it is recommended that average buoyancy forces are estimated by using an average temperature difference of +5 or +30 °C between the cavity air and outdoor air. Depending on the angle between the considered wall cladding and the predominant wind direction, the ventilation potential is calculated assuming the wind-induced force to either assist or counteract the buoyancy-induced force. In the synthesis report of the above mentioned R&D project, Burnett et al. [60] argue that for cladding systems which are primarily ventilated by vertical pressure gradients, buoyancy-forces are probably more common and more consistent than wind-forces.

Paper III

Approach to predict cavity ventilation rates

Paper III presents calculations of hourly ventilation rates in the experimental walls using hourly solar radiation and wind speed field data. In the approach to convert hourly climate data into ventilation rates, ventilation rate is expressed as a function of wind speed and global vertical solar radiation, respectively. For 13 different time periods extending from 24 to 91 hours, the calculated average ventilation rates were within or very close to the experimentally estimated limits for the average ventilation rates presented in *Paper I*. Additionally, the calculations captured the temporal variability and physical cause of ventilation airflow in the cavities reasonably well. The demonstrated methodology has the potential to be developed into a user friendly approach to determine realistic hourly and average cladding ventilation rate input data for hygrothermal simulation purposes.

In the present study, evaluation of the cavity air velocity measurements performed in the experimental walls indicated a very complex and unpredictable action of wind-induced cavity airflow due to constantly changing wind pressure conditions at the cavity openings (*Paper I*). Thus, modelling of the combined effect of wind and buoyancy is difficult to perform and therefore a simple driving force model was suggested (*Paper II*). In the model, thermal buoyancy pressures and wind pressures are not combined and daytime ventilation is considered to be solely buoyancy driven. Using the driving force model and tabular climate data, calculations of average ventilation rates in the experimental walls for a 5 month period compared favourably with experimental findings (*Paper II*). However, since wind data but no solar radiation data was collected during the cavity air velocity measurements, comparative calculations based on the actual climatic conditions during the field measurement period were not performed. Therefore, it was not confirmed that the driving force model actually captured the physical cause of the cavity airflow. In *Paper III*, radiation data collected by Larsson [61] at the time of the cavity air velocity measurements was used to calculate hourly cavity ventilation rates for comparison with the previous experimental results. Results from one of the investigated time periods in cavity 4 are shown in Figure 15.
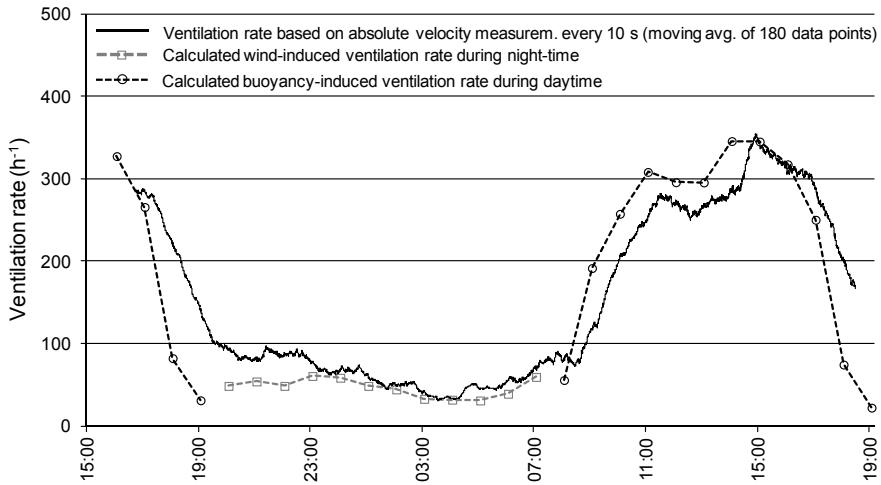
Figure 15.
Calculated hourly buoyancy-induced (black dashed lines) and wind-induced (gray dashed line) ventilation rates in the experimental wall cavity 4 (Figure 12) compared with a moving average (solid black line), determined from cavity air velocity measurements (*Paper I*). For performing calculations of the buoyancy induced daytime ventilation, solar radiation data from Larsson [61] was used. Furthermore, calculations of the wind-induced ventilation during night-time were supported by experimental findings regarding the exterior pressure difference coefficient (*Paper I*). The timing difference between the calculated and experimentally determined buoyancy-driven ventilation is attributed to the heat capacity of the wall materials.

Cladding deformations

Background to the study

A rendered rainscreen cladding is a multilayer system where materials with different properties are combined and bonded to each other to mechanically interact. By means of an intermediate structural support system (Figure 2), the rainscreen is connected to the underlying wall structure. In Figure 16, a sequence of pictures taken during the construction of the experimental walls (Figure 12) shows the stages of multilayer rainscreen assemblies.
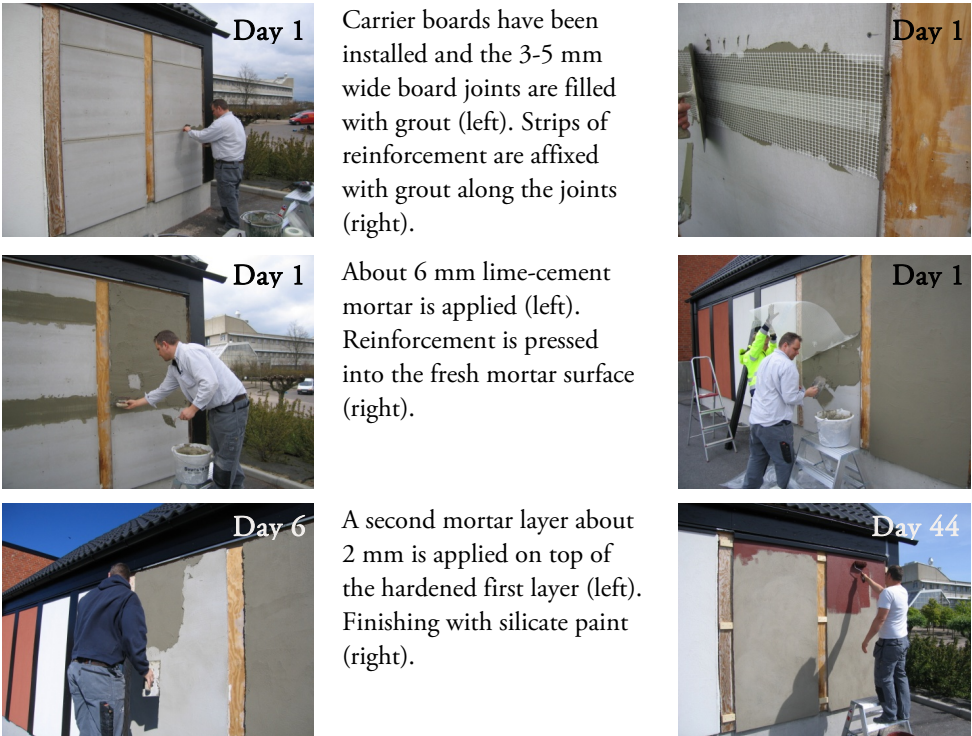

Carrier boards have been installed and the 3-5 mm wide board joints are filled with grout (left). Strips of reinforcement are affixed with grout along the joints (right).

About 6 mm lime-cement mortar is applied (left). Reinforcement is pressed into the fresh mortar surface (right).

A second mortar layer about 2 mm is applied on top of the hardened first layer (left). Finishing with silicate paint (right).

Figure 16.
Construction of the rendered screen used on the experimental walls. Materials and details of the screen installation shown in the figure differ from other commercially available systems. In the present research project, deformations were not measured in the experimental walls.

Immediately after assembly, cladding deformations may develop due to initial render and board drying shrinkage. Later on during operating conditions, deformations are caused by repeated changes in cladding temperature and moisture content. Due to internal and external restraint to deformations, stresses are induced in the cladding. In addition, cladding stresses are induced by wind pressure and dimensional instability of the support system and backup wall structure. Potentially, the stresses may exceed the strength of the cladding materials and cause a variety of defects such as cracks, spalling and separation between layers. If defects occur, cladding aesthetics and durability can be adversely affected. An example of a rendered rainscreen suffering severe degradation is shown in Figure 17. It should be emphasised that the present study has not been initiated by a poor track record of rendered screens. However, the bad experience with ETICS clearly shows the importance of understanding the technical features and limitations of specific system approaches before large-scale implementation to avoid subsequent costly repairs.

Figure 17.
For this rendered rainscreen in the south of Sweden, signs of degradation were visible shortly after completion. Details of the screen and wall design have not been investigated in this study and the picture is shown for illustration purposes only.

Paper IV

Measurements of moisture-induced cladding deformation

Paper IV presents measurements of elastic moduli, vapour diffusion coefficients, moisture fixation properties and moisture expansion characteristics of carrier boards and renders that are used in two different commercially available rainscreen cladding compositions. In an experimental set-up, board specimens with and without render were exposed to changing moisture conditions and the free in-plane and out-of-plane deformations were measured. The experimental results were compared with deformation calculations based on a simple mechanical two-layer model. For the out-of-plane deformations, the correlation between the experimental results and the calculations were poor. First, unexpected and significant deformations occurred due to creep and cracking. In view of this, the design of the experimental set-up in which the influence of gravity not was eliminated was inappropriate. Second, the mechanical model did not take into account the effect of multiple glass fiber meshes in the studied compositions. The results showed that their influence on the out-of-plane deformation behaviour is significant.

In order to analyse the mechanical behaviour of full-scale rainscreen assemblies, it is required to consider the:

(1) physical properties of individual screen layers as a function of time, moisture and temperature

(2) mechanical interaction between the screen layers and between the screen and the underlying structure

(3) effects of autogenous shrinkage and initial drying shrinkage

(4) effects of wind, air temperature, air humidity, rain and solar radiation

The present study was limited to laboratory investigations of the free in-plane and out-of-plane deformation behaviour of two commercially available rainscreen compositions under changing moisture conditions. It should be noted that strains and stresses in claddings exposed to changing moisture conditions are described in essentially similar terms to those used for determination of thermally induced strains and stresses.

During the 90's, it was observed that many mineral renders used in ETICS installations suffered severe cracking. Therefore, a problem inventory was performed

by Sandin [62] and based on this, a research project was initiated. In the project, the characteristics of typical lime-cement renders used on thermal insulation were investigated [63-69] and, among other things, a laboratory set-up was developed to study the moisture-induced deformation behaviour [66]. In the present study, the set-up was used for measurements of moisture-induced composite cladding deformations (*Paper IV*).

Temperature and relative humidity measurements

The mechanical performance of rendered rainscreen cladding assemblies on real walls was not modelled in this study. However, for the purpose of investigating how air temperature, air humidity and solar radiation influence the conditions in a south oriented cladding, cladding temperatures and relative humidity boundary conditions were measured in the experimental walls (Figure 12). The specific questions that motivated the measurements were:

- annual and daily cladding temperature and relative humidity ranges ?

- shape of temperature and relative humidity gradients across the cladding ?

- significance of cavity ventilation for the cladding conditions ?

The field measurement data presented in the following were collected during a period from mid June to mid February. For data collection, the outdoor climate and all four experimental walls were monitored. Nevertheless, primarily the results for cavity 1 and 2 are presented and discussed since the different cladding support systems used in these two cavities resulted in maximum and minimum cavity ventilation. So, differences due to cavity ventilation are highlighted.

Temperature

Cladding temperatures were measured every 15 minutes using (type) Pentronic T thermocouples. In the vertical centre axis of each cavity, three sensors were installed at cladding mid-height as follows:

- in the board back surface

- in the board–render interface

- close to the render surface

Positioning of the sensors is shown schematically in Figure 19. In addition to mid-height cladding temperatures, cavity air temperatures were measured with vertical arrays of three thermocouples (Figure 12).

Based on the data from the three temperature sensors across the cladding in front of the "non-ventilated" cavity 2, Figure 18 shows the average cladding temperature T_{avg} (°C).
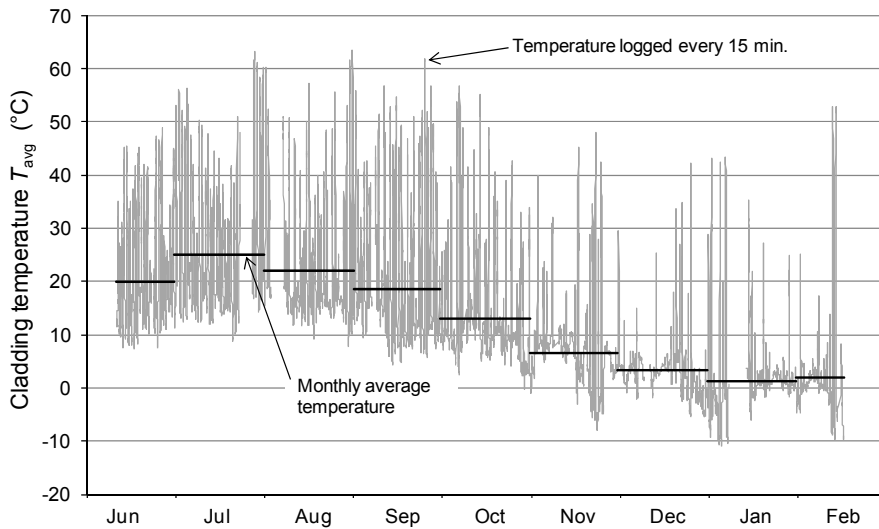

Figure 18.
The transient and monthly average temperatures across the cladding in front of the "non-ventilated" cavity 2. For June and February, the temperature data refers only to parts of the months. In addition, data is missing for some periods from July to January. For the ventilated cavity 1 cladding, the monthly average temperatures evaluated from the measurements across the cladding were insignificantly lower.

Figure 18 shows that the extreme monthly average cladding temperatures, 25.1 and 1.3 °C, occurred in July and January, respectively. Concerning the ventilated cavity 1 cladding, the corresponding temperatures in July and January were 24.4 and 0.8 °C, meaning that the impact of cavity ventilation on the monthly average cladding temperatures was insignificant.

The daily temperature ranges in the cavity 2 cladding were large, see Figure 18. Maximum average cladding temperatures, 62–63 °C, occurred in July–September and minimum temperatures, -10 °C, occurred in January and February. Accordingly, the annual temperature range in the "non-ventilated" cladding was approximately 73 °C.

In comparison, the annual temperature range in the ventilated cladding was lower, about 67 °C, since the maximum average cladding temperature not exceeded 57 °C.

The maximum daily temperature range, 63 °C, was reached on February 13. Figure 19 presents a detailed comparison of the temperature distributions across the cavity 1 and 2 cladding in the heating and cooling phase during this specific day. While the average temperature across the "non-ventilated" cladding peaked at 53 °C, the cavity 1 cladding only experienced 41 °C due to the ventilation cooling effect. It can be added that at the peak cladding temperatures, the cavity air temperature at mid height was 14 and 50 °C in cavity 1 and 2, respectively.
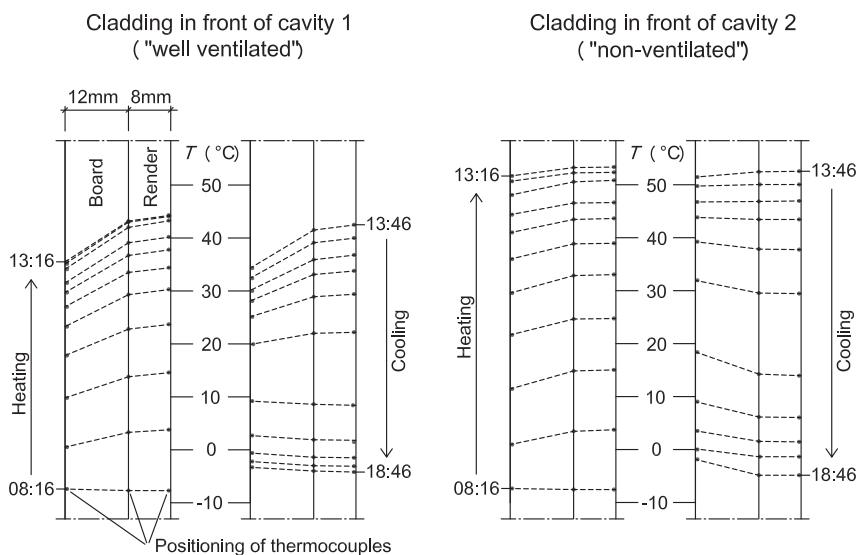

Figure 19.
Non-steady state cladding temperatures on February 13 for time intervals of 30 minutes. Between the thermocouples, the temperature gradient is indicated as linear but due to the heat capacity of the board and render, the true gradient is not entirely linear.

Considering the temperature distributions shown in Figure 19, the maximum gradient across the cavity 1 cladding, 9–10 °C, was reached in the heating phase at 12:16. In the cavity 2 cladding, the maximum gradient, 4-5 °C, occurred in the cooling phase at 16:46. For the entire measurement period, temperature gradients comparable to those shown in Figure 19 developed repetitively in the claddings, but the gradients on February 13 were the largest.

Since the airflow in cavity 1 on February 13 was an effect of solar radiation, the cavity air temperature gradually increased along the height of the cavity. Accordingly, the

maximum temperature gradient across the cavity 1 cladding close to the bottom and top of the cladding was somewhat larger and smaller, respectively, than that at mid-height.

Relative humidity

Relative humidity (RH) of the cavity air was measured with vertical arrays of three calibrated sensors (type) Vaisala HMP44 (Figure 12). The RH data presented in the following refers to the sensors positioned at mid-height. Note that no measurements of relative humidity were performed in the cladding.

To facilitate understanding of the results, the measured monthly average cavity air and outdoor temperatures are presented in Figure 20.
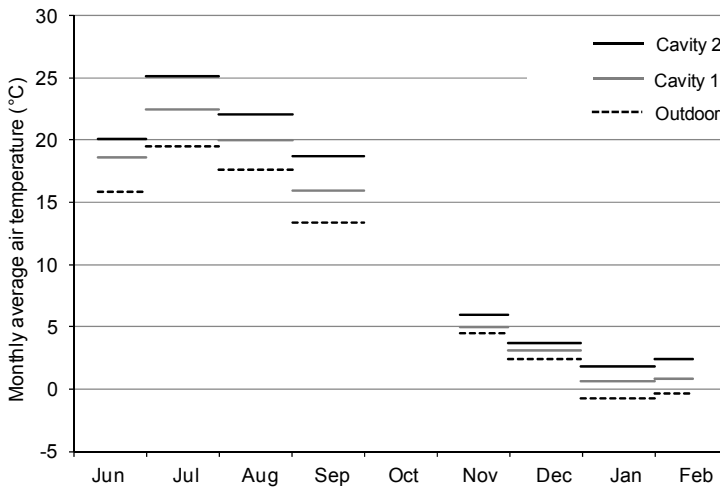
Figure 20.
Air temperatures determined in the field measurements. The cavity air temperatures refer to temperature sensors positioned at mid-height.

Results from the RH measurements are presented in Figure 21, arranged as follows:

- 21a shows the transient RH data for cavity 1 including monthly averages
- 21b shows the corresponding results for the "non-ventilated" cavity 2
- 21c presents the outdoor RH data including the monthly average data from figure 21a and 21b
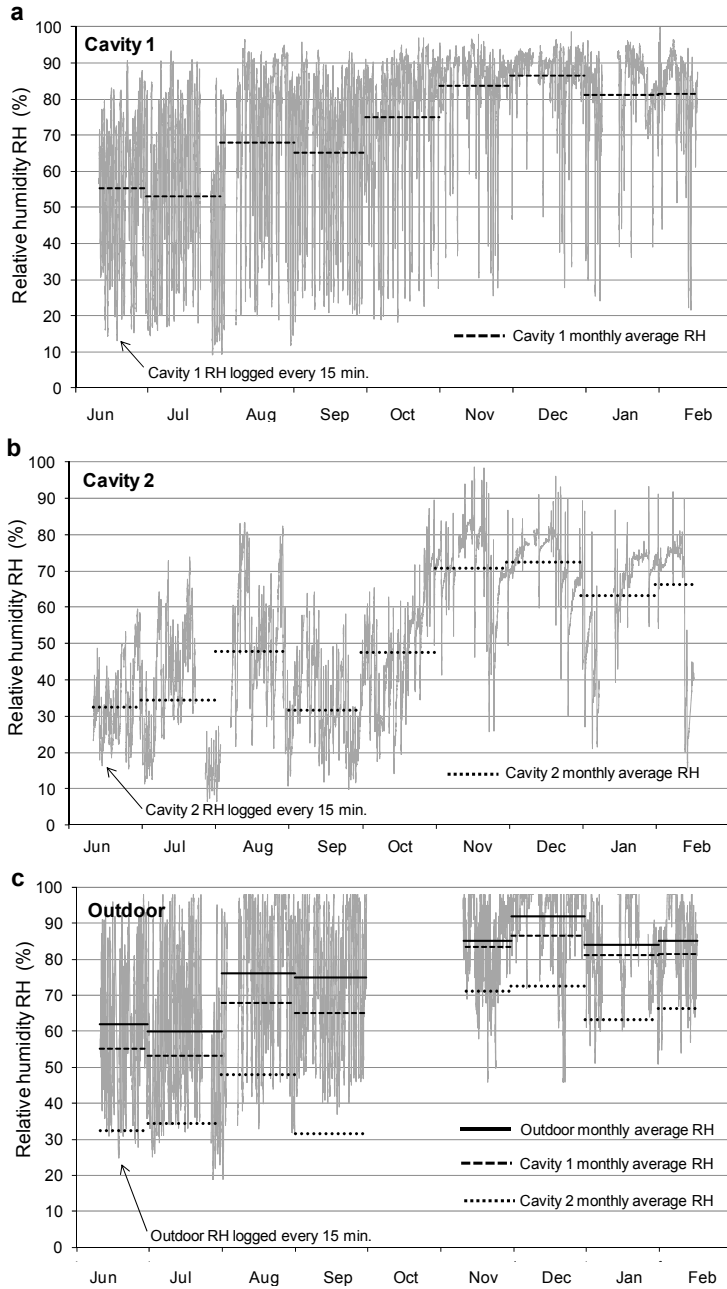
Figure 21.
Results from measurements of RH in cavity 1 (a), in cavity 2 (b) and in the outdoor air (c). The lack of outdoor RH data for most of October and parts of November was due to malfunction of the weather station.

By combining the average data given in Figures 18, 20 and 21c, the RH conditions at the cladding front and back surfaces were calculated, giving an annual RH range across the cavity 1 and 2 cladding of about 50–90% and 40–80%, respectively. Considering monthly average RH gradients across the claddings, the cavity 1 cladding gradient was generally small, less than 5% RH, whereas the "non-ventilated" cladding gradient was in the interval 5–15% RH except for September where it reached 23% RH.

It should be emphasised that the boundary condition measurements excluded the impact of rain and surface condensation, acting for increasing the cladding RH in the winter months. Additionally, continuous periods in the summer months with highly elevated daytime cladding temperatures may have a strong drying effect on the cladding. Consequently, the annual RH ranges presented above are underestimates.

For estimating the effect of the daily temperature fluctuations on the monthly average cladding RH, calculations of RH distributions in July were performed using the computer program KFX03 [70], monthly average values of the daytime (08-20) and night-time (20-08) cladding surface temperatures and average daytime and night-time vapour content of the air at the cladding front and back boundary. Furthermore, the calculations used realistic moisture fixation and vapour permeability data for the board and render (*Paper IV*). In Figure 22, the daily RH distributions in July are compared with the monthly RH averages.
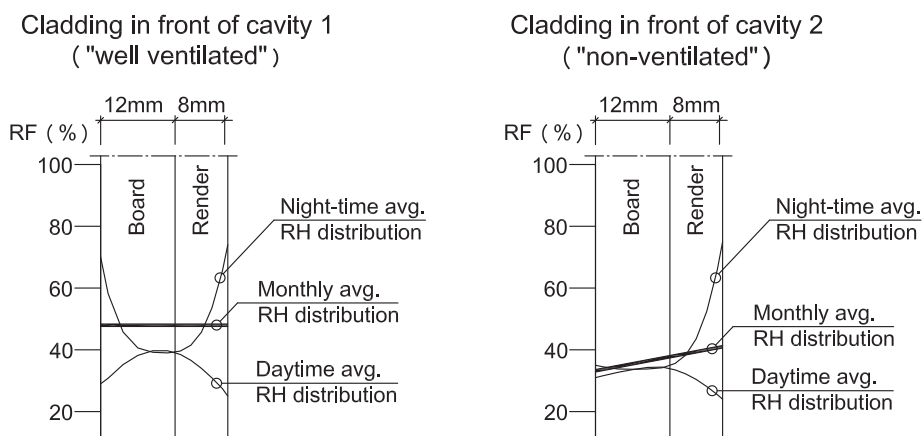

Figure 22.
Calculated daily RH distributions across the claddings in July in consideration of temperature fluctuations. The monthly average RH distributions (straight lines) were determined using the monthly average data shown in Figures 18, 20 and 21c.

Focusing on the ventilated cladding, Figure 22 shows that the daily temperature fluctuations had the effect of decreasing the average RH in July by about 10% RH. Thus, the annual RH range was at least 40-90%. Notwithstanding that the average daytime and night-time RH distributions shown in the figure are not the fully developed extremes; the distributions suggest that daily variations at the boundaries caused steep but quite symmetrical cladding RH gradients.

For the "non-ventilated" cladding, the results in Figure 22 indicate that the daily temperature fluctuations decreased the average RH by less than 5% RH, increasing the annual range to at least 35-80% RH. In contrast to the ventilated case, the cavity 2 distributions show that the absence of ventilation introduced a distinctive unsymmetrical night-time RH distribution across the cladding.

The monthly average RH conditions in the cavity 1 air (Figure 21a) agree fairly well with calculations based on the average outdoor RH data (Figure 21c) and the average outdoor and cavity air temperatures (Figure 20). Since the RH of air decreases if the temperature increases, the drier conditions in the "non-ventilated" cavity agree with the results in Figure 20, showing that the temperature of the cavity 2 air was higher than that of the cavity 1 air. However, the RH of the "non-ventilated" air was consistently lower than the temperature conditions explain. For example, the average RH in September was measured to be 32% (Figure 21b) whereas calculations based on the outdoor climate and the cavity air temperature give an expected RH of 54%. To investigate the cause of this large discrepancy, Figure 23 shows the average vapour content of the air in cavity 1–4 in September, evaluated from the measurement data. In addition to the mid-height position, the figure includes the two measurement positions close to the cavity top and bottom.
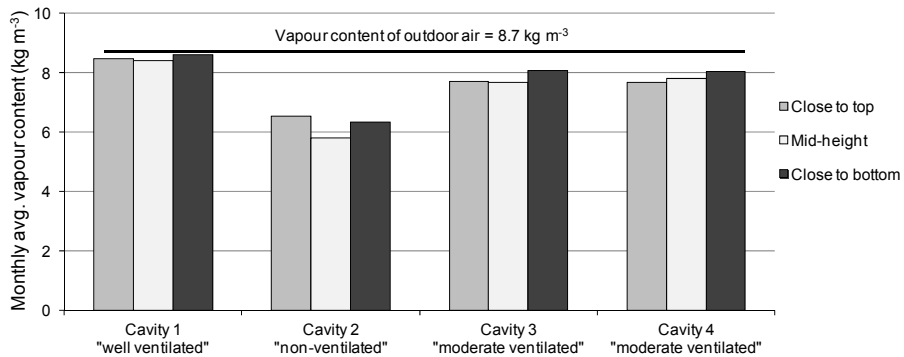

Figure 23.
For three different positions in cavity 1–4, the figure gives a comparison of the monthly average vapour content of the cavity air and outdoor air in September.

From Figure 23, it is clear that the vapour content of the cavity 2 air was considerably lower than that of the outdoor air at all three measurement positions. In addition to this, the figure shows that the vapour content of the cavity air correlated with the ventilation rate. These observations support the validity of the measurement data, but the mechanism causing large vapour content differences between the outdoor air and cavity air is not obvious. To provide a physical explanation for how such conditions can occur, Figure 24 gives some qualitative distributions of relative humidity, vapour content and temperature across the "non-ventilated" cavity and cladding during a day with solar heating. It is assumed that the initial distributions are uniform and that the cladding consists of a single layer.
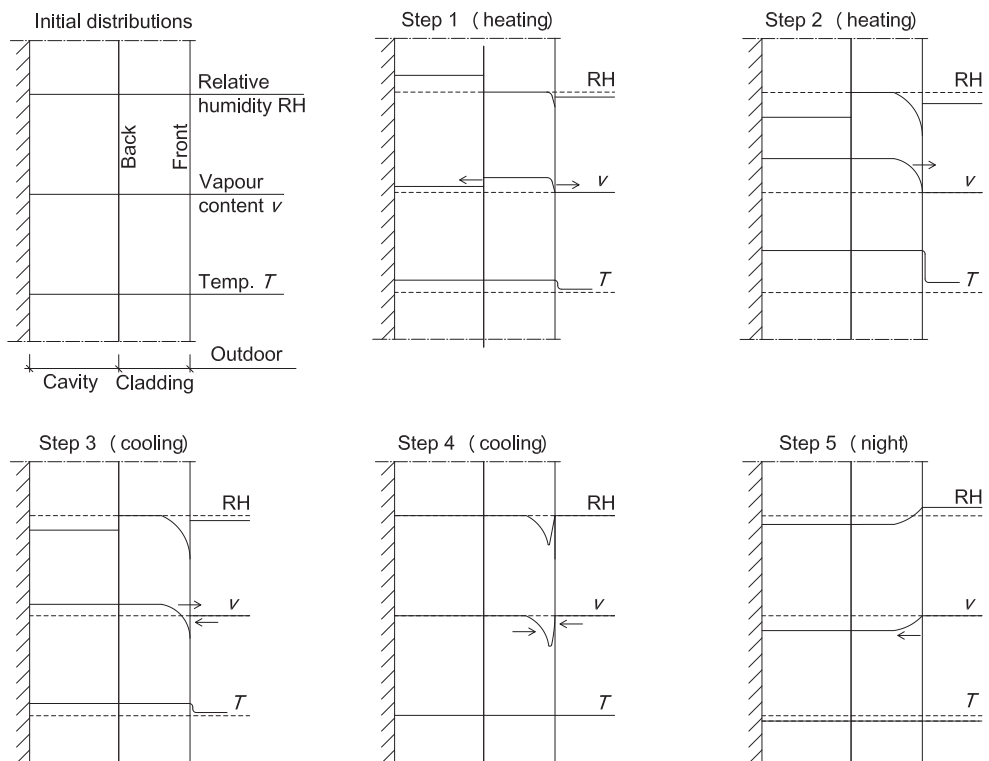

Figure 24.
Qualitative distributions of RH, vapour content and temperature across a "non-ventilated" cavity and cladding for conditions with daytime solar heating. The arrows indicate the direction of moisture flow.

For the understanding of Figure 24, some detailed comments are motivated:

Step 1   Solar radiation starts to heat the wall and the temperature of the cladding and cavity air increase. The temperature increase causes the vapour content in the cladding pore system to increase, initiating an inward and outward moisture flow. The RH in the cladding is unaffected since the vapour content and saturation vapour content in the cladding pore system increase simultaneously and equally as the temperature increases. However, due to the outward moisture flow, the cladding dries and a vapour content and RH gradient starts emerging in the cladding front. In the cavity air, the effect of increased temperature and vapour content is that the RH of the cavity air increases (that this is the case is supported by field measurement results which are not shown).

Step 2   The cladding and cavity air temperature peak. Consequently, the vapour content in the cladding pore system peaks. The cladding has continued to dry outwards and the vapour content and RH gradient in the cladding front have increased. Since the moisture capacity of the cavity air is small compared with the moisture capacity of the cladding, the inward moisture flow shown in step 1 has not resulted in any significant drying of the cladding. In addition, the vapour content of the cavity air is controlled by the vapour content in the cladding pore system. The RH of the cavity air has dropped due to a substantial increase in the cavity air temperature (supported by field measurement results which are not shown).

Step 3   The temperature starts decreasing and as a consequence, the vapour content and saturation vapour content in the cladding pore system decrease. Due to the temperature drop, the vapour content in the cladding pore system at the front surface now drops below the vapour content of the outdoor air. Accordingly, moisture starts flowing towards the front of the cladding from two directions. The RH in the cladding is initially unaffected by the temperature decrease. In the cavity air, the effect of decreased temperature and vapour content is that the RH of the cavity air increases (supported by field measurement results which are not shown).

Step 4   The initial temperature distribution is regained. In the front of the cladding, the moisture flow from two directions has the effect of equalising the vapour content and RH gradient. In the process, moisture is redistributed from the back part of the cladding towards the front.

Step 5   The cladding redistribution process is finished and as a result, the vapour content in the cladding pore system and cavity air is lower than that of the outdoor air. At the cladding front, the inward moisture flow continues.

The qualitative analysis shows that it is possible for the vapour content of the cavity air to drop below levels of the outdoor air. For quantitative determinations of long-term vapour content differences between the cavity air and outdoor air, a more sophisticated analysis method than that demonstrated in Figure 24 is required.

It should be borne in mind that the design of the experimental walls only allowed for vertical airflow in the cavities. However, in real cavities designed with horizontal metal battens, wind pressure differences may induce both horizontal and vertical airflow. This means that the observed phenomenon with large vapour content differences between the cavity air and outdoor air may be less pronounced in practice than in the experimental walls.

Potential for in-plane deformations

Temperature and moisture content changes cause in-plane cladding deformations. In addition, temperature and moisture content gradients across the cladding cause out-of-plane deformations. For assemblies consisting of bonded layers which cannot deform independently, out-of-plane deformations can also take place as a result of uniform temperature and moisture content changes due to differential expansion between the individual layers.

Using the results from the presented field measurements in the experimental walls, the potential for thermal and moisture-induced in-plane deformations of the cladding on these walls can be demonstrated. For this purpose, Table 4 gives coefficient of thermal expansion data and moisture expansion data (*Paper IV*) for the board and render used in the cladding.

Table 4.
Coefficient of thermal expansion data and moisture expansion data for the carrier board and render used in the cladding on the experimental walls.

Material layer	Coefficient of thermal expansion $(\cdot 10^{-6} \ ^{\circ}C^{-1})$	Moisture expansion (‰)
Carrier board	7[*]	0.5[***]
Lime-cement render	7–10[**]	0.4[***]

[*]Manufacturer data, [**] From Nevander et al. [32] [***]RH interval 30-90% (*Paper IV*)

In the continued presentation, the coefficient of thermal expansion of the render is taken to be $10 \cdot 10^{-6} \ ^{\circ}C^{-1}$.

Generally, the determination of the magnitude of a deformation means determining the difference between two deformation states, one of which constitutes a reference

state. Preferably, the reference state corresponds to the temperature and relative humidity conditions during construction of the cladding.

In the following, it is assumed that the cladding on the experimental walls was assembled in October. Based on climate data presented in Nevander et al. [32] the monthly average conditions in the outdoor air at this time of year can be estimated to be 9 °C and 90% RH. So, this temperature and RH defines the reference state.

According to the data shown in Table 4, the board and render exhibit differences in both thermal expansion and moisture expansion. For this reason, the deformations presented below were determined using Figure 3 shown on page 7 in *Paper IV*. In addition, data concerning the modulus of elasticity of the board and render given in Table 3 on page 12 in the mentioned paper were used.

Starting with the thermal in-plane deformations, the measured annual temperature range, 73 °C, in the "non-ventilated" cladding is equivalent to a total in-plane deformation of 0.60‰. Relative to the reference state, the maximum expansion and contraction is 0.44 and 0.16‰, respectively. The expansion of the ventilated cladding is somewhat lower, 0.40‰. The maximum thermal expansions occur in July–September.

The annual RH range for the "non-ventilated" cladding was estimated to be 35-80%. Therefore, the cladding experiences moisture-induced contraction throughout the year. The maximum contraction, 0.42‰, occurs in June–July. Since the ventilated cladding only dries to about 40% RH, its corresponding contraction is 0.38‰.

In the presented scenario, the maximum thermal expansions occur during daytime in summer and happen to be close to the moisture-induced contractions at this time of the year. Consequently the magnitude of the resulting in-plane deformations of the claddings during daytime is small. However, the measurement results presented in Figure 18 indicate that the temperature of the claddings drops to about 10 °C during night-time in summer which implies that the maximum contractions occur. Considering the simulated night-time RH distributions across the claddings in July (Figure 22), the magnitude of the maximum contraction of the "non-ventilated" and the ventilated cladding can be estimated to be 0.35 and 0.25‰, respectively. In contrast to the ventilated case, Figure 22 shows the night-time moisture-induced contraction of the "non-ventilated" cladding coincides with a very unsymmetrical RH distribution across the cladding, causing out-of-plane deformations.

Conclusions and future studies

Conclusions

The main objective of this thesis was to investigate relationships between cavity design, ventilation rate and ventilation drying. For this purpose, laboratory measurements, full-scale field testing in experimental walls and modelling have been performed. Special attention has been paid to the investigation of differences depending on two types of support systems that often are used in practice – vertical wooden battens and perforated horizontal metal battens. The conclusions based on the investigations and the results from the appended papers are summarised below.

Field tests of air velocities and air temperatures in the cavities of the experimental walls were made using a thermal anemometer and vertical arrays of thermocouples (*Paper I*). In order to estimate ventilation rates and evaluate the characteristics of driving forces, the experimental data were compared with a physical cavity airflow model. The main findings were:

(1) With vertical wooden battens, the average ventilation rate during October–February was estimated to be 230–310 h^{-1}. In the cavities with horizontal metal battens, it was about 100 h^{-1}. Relations between the average ventilation rates in the different cavities were roughly in agreement with predictions based on the airflow model.

(2) The ventilation rates showed considerable temporal variability. The highest observed ventilation rates were induced by thermal buoyancy and occurred during daytime hours when the sky was clear.

(3) The magnitude of the forces driving airflow was small, less than 0.2–0.3 Pa during 50% of the time and less than 0.1 Pa during 30–40% of the time. Driving forces larger than 2 Pa occurred less than 5% of the time.

(4) Wind-induced airflow in the cavities was irregular with frequent changes in both velocity and direction, independent of the incident wind angle. The frequent changes in direction significantly reduced the efficiency of wind-driven airflow to exchange the air in the cavities.

(5) An exterior pressure difference coefficient (ΔC_p) in the interval of 0.025–0.05 was applicable to estimate wind-driven ventilation rates when wind forces acted in the absence of thermal buoyancy.

(6) When strong buoyancy-driven airflow was established in the cavities, wind-induced airflow was suppressed. This mode of action was particularly clear in the cavities with horizontal metal battens since these battens introduce a steep incline in the curve describing the relationship between driving force and airflow.

Average ventilation rates in the experimental walls were calculated and converted into drying rates during three different phases of the ventilation drying process (*Paper II*). The calculations were performed using:

- the cavity airflow model

- a simple driving force model

- models of cavity heat balance and moisture balance

- monthly and annual tabular climate data

The numerical changes in the ventilation and drying rates depending on changes in the cavity design and season were investigated in a parametric study. The main conclusions were:

(1) For the actual design of the experimental walls, the calculated average ventilation rates during October–February were in good agreement with the experimental findings presented in *Paper I*, indicating that the driving force model was a reasonable approach to predict ventilation rates in the experimental walls.

(2) The cavity design is of great importance for ventilation drying rates if the material in the direct vicinity of the cavity is wet over its entire extent and drying occurs by evaporation to the cavity air. For such extreme conditions, a light façade colour, horizontal metal battens and, in particular, a small cavity depth, are adverse factors for drying rates.

(3) When evaporation ceases and the continued moisture removal from the material to the cavity air becomes dependent on vapour diffusion, drying rates for different cavity designs tend to be evened out. If the resistance to vapour flow in the material reaches high levels ($Z_v = 50 \cdot 10^3$ s m^{-1}), a favourable outdoor climate is significantly more important than the cavity design for promoting ventilation drying.

The practical implications of the derived ventilation drying rates were demonstrated in calculations of drying times for sheathing of gypsum (*Paper II*). The sheathing was assumed to be initially wet over its entire extent and installed in the direct vicinity of the cavity. The calculations showed that:

(1) The drying time is longer with horizontal metal battens compared with vertical battens. But, if the geometric conditions at the cavity openings follow practical design, whereby the flow areas at the openings are reduced compared with the cavity cross section area, the difference in drying time is insignificant.

(2) An increase of the cavity depth from 25 to 40 mm only reduces the drying time marginally. However, a decrease of the cavity depth from 10 to 5 mm extends the drying time by a factor 5.

(3) The drying time is extended by a factor 2 or more if the cladding absorptivity for solar radiation changes from 0.9 (dark colour) to 0.25 (light colour).

Drying time calculations were additionally performed assuming the wet area of the sheathing to be rectangular shaped with a height of 50 mm and with a horizontal extension equal to the width of the cavity (*Paper II*). For this wetting event, the calculations showed that the most adverse factor for the drying time is a light façade colour whereas differences in the drying time depending on the cavity depth are small.

For comparison with the experimental results presented in *Paper I*, calculations of hourly ventilation rates using the simple driving force model and high-resolution solar radiation and wind speed field data were performed (*Paper III*). For converting the field data, the airflow and heat balance models were used to express the cavity ventilation as a function of solar radiation and wind speed, respectively. The findings were:

(1) For 13 individual time periods extending from 24 to 91 hours, the calculated period average ventilation rates compared favourably with estimates based on the results from the cavity air velocity measurements.

(2) On an hourly basis, the calculations captured the temporal variability and the physical cause of ventilation airflow in the cavities reasonably well. However, large hourly deviations occurred during daytime hours with weak buoyancy pressure compared with wind pressure, indicating that the driving force model can be improved by adding a criterion for when the buoyancy pressure is insignificant compared with the wind pressure.

The calculation methodology presented in *Paper III* can be developed into a user friendly approach to model realistic ventilation rate input data for hygrothermal simulation purposes. In a modelling demonstration which used the methodology and hourly wind speed and solar radiation data provided by the Swedish Meteorological and Hydrological Institute, it was found that:

(1) The modelled monthly ventilation rates during October–February were in good agreement with the experimental estimations presented in *Paper I*.

(2) Differences between modelled annual average ventilation rates for 8 different years (1991–1998) were small.

A second objective of this thesis was to investigate how two commercially available rainscreen claddings composed of composite carrier boards and renders are deformed on exposure to moisture changes. For this purpose, laboratory experiments and

modelling using a simple mechanical two-layer model have been performed (*Paper IV*). The main findings from these studies were:

(1) The results obtained in the measurements of moisture fixation properties and moisture expansion characteristics indicated that soaking in water and drying in oven (60 °C) induced changes in the physical properties of the composite boards. The effects of such changes in the material properties should be considered when modelling the deformations that occur in full-scale rainscreen assemblies under real conditions.

(2) Modelling of out-of-plane deformations of the composite boards requires that the individual material properties, such as elastic modulus and moisture expansion, of the matrix and the surface meshes are known. This implies that the mechanical model must be extended to handle more than two layers. Such an extension of the model is even more important for predicting out-of-plane deformations of boards with render since the render includes an additional mesh.

Future studies

The presented study of cavity ventilation rates and ventilation drying has only been concerned with one-storey high walls. On multi-storey buildings, wall cavities are usually designed to be continuous from ground level to roof level. More studies are needed to investigate the relative importance of wind-induced and buoyancy-induced airflow for the ventilation process of such cavities.

In the experimental walls, the design only allowed for vertical cavity airflow. In an actual façade, cavity airflow in all directions is possible if the support system consists of horizontal metal battens. Investigations of the importance of such airflow are a remaining task.

The experimental validation of the investigated methodology for the prediction of cavity ventilation rates was limited to small, south oriented walls with a specific design on a specific geographic location. To investigate if predictions based on the methodology are valid for other conditions, further on-site experiments are necessary. It is recommended that such experimental studies include walls with different orientation, height and façade colour as well as varying outdoor conditions.

The cladding deformation study was limited to laboratory experiments and modelling using a mechanical two-layer model based on simplified assumptions. Among the remaining tasks towards a better understanding of the deformation behaviour of rendered rainscreen claddings are:

- extended investigations of how the material properties of the studied cladding components changes when they are exposed to elevated temperatures and repeated wetting and drying. Studies should also be performed focusing on analysing the overall aging process of the materials.

- to develop the mechanical model so that the effects of multiple glass fiber meshes can be taken into account. For validation of the model, a modified experimental set-up where the influence of gravity is eliminated should be used.

- to investigate the magnitude of deformations that occur in the early stages due to autogenous shrinkage and initial drying shrinkage.

- to perform field measurements of deformations that occur in real cladding assemblies for comparison with calculations.

References

[1] Straube J, Burnett EFP. Rain control and design strategies. Journal of Building Physics. 1999;23:41-56

[2] Lundell H. Historien bakom träpanelens luftspalt (The history of the air gap behind wood panel). Examensarbete E-93:3. Göteborg: Chalmers Tekniska Högskola 1993. (in Swedish).

[3] Samuelson I, Jansson A. Putsade regelväggar (Rendered stud walls). SP report 2009:16. Borås: SP Energiteknik; 2009. (in Swedish).

[4] BBR. Regelsamling för byggande, BBR 2012 (Building regulations, BBR 2012). Boverket; 2012. (in Swedish).

[5] Elmarsson B. Puts på tilläggsisolering (Render on external supplementary insulation). T5:1979. Stockholm: Statens råd för byggnadsforskning; 1979. (in Swedish).

[6] Hagman F. Puts som ytskikt på mineralull och cellplast (Render as a surface layer on mineral wool and cellular plastic). R8:1978. Stockholm: Statens råd för byggnadsforskning; 1978. (in Swedish).

[7] Elmarsson B, Nevander LE. Puts på tilläggsisolering (Render on external supplementary insulation). TVBH-3001. Lund: Division of Building Technology; 1978. (in Swedish).

[8] Elmarsson B. Puts på tilläggsisolering - Serporockmetoden (Render on external supplementary insulation - The Serporock method). TVBH-3010. Lund: Division of Building Technology; 1983. (in Swedish).

[9] Elmarsson B. Puts på tilläggsisolering (Render on external supplementary insulation). R120:1984. Stockholm: Statens råd för byggnadsforskning; 1984. (in Swedish).

[10] Cheple M, Huelman PH. Literature Review of Exterior Insulation Finish Systems and Stucco Finishes. Cold Climate Housing Progam. University of Minnesota. 2000.

[11] Künzel M, Zirkelbach D. Influence of rain water leakage on the hygrothermal performance of exterior insulation systems. In: 8th Symposium on Building Physics in the Nordic Countries. Copenhagen. 2008.

[12] Jansson A, Samuelson I, Mörnell K. Skador i putsade träregelväggar (Damages in rendered wood frame walls). Bygg & Teknik no 1 2007. (in Swedish).

[13] Jansson A. Putsade regelväggar 2011 (Rendered stud walls 2011). SP report 2011:61. Borås: SP Energiteknik; 2011. (in Swedish).

[14] Rousseau MZ. Facts and fictions of rain screen walls. Construction Canada 90 03. 1990;32:40-7

[15] Rousseau MZ, Poirier GF, Brown WC. Pressure equalization in rainscreen wall systems. NRC-CNRC Construction Technology Update No 17: Institute for Research in Construction; 1998.

[16] Kumar KS. Pressure equalization of rainscreen walls: a critical review. Building and Environment. 2000;35:161-79

[17] MCA. Understanding "the rainscreen principle". Glenview, IL: Metal Construction Association; 2006.

[18] TenWolde A, Carll C, Malinauskas V. Airflows and moisture conditions in walls of manufactured homes. Airflow Performance of Building Envelopes, Components and Systems, ASTM STP 1255 Mark P Modera and Andrew K Persily, Eds, American Society for Testing and Materials, Philadelphia. 1995:137-55

[19] Bassett M, McNeil S. Ventilation measured in the wall cavities of high moisture risk buildings. Journal of Building Physics. 2009;32:291-303

[20] Hagentoft CE. Introduction to Building Physics. Lund: Studentlitteratur; 2001.

[21] ASHRAE. ASHRAE Handbook - Fundamentals. Atlanta, GA: American Society of Heating, Refrigerating and Air-Conditioning Engineers; 2001.

[22] Burnett EFP, Straube J. Vents, ventilation drying and pressure moderation. Ottawa: Building Engineering Group, University of Waterloo; 1995.

[23] Uvsløkk S. The importance of wind barriers for insulated timber frame constructions. Journal of Thermal Insulation and Building Envelopes. 1996;20:40-62

[24] Gudum C. Moisture Transport and Convection in Building Envelopes - Ventilation in Light Weight Outer Walls [PhD Thesis]. Lyngby: Technical University of Denmark; 2003.

[25] Sandin K. Skalmurskonstruktionens fukt- och temperaturbetingelser (Moisture- and temperature conditions in brick veneer walls). Stockholm: Byggforskningsrådet; 1991. (in Swedish).

[26] Piñon J, Davidovic D, Burnett E, Srebric J. Characterization of Ventilation Airflow in Screen-Type Wall Systems. ASHRAE 1091 - Report #5. The Pennsylvania Housing Research/Resource Center. The Pennsylvania State University; 2004.

[27] Bejan A. Heat transfer. New York: John Wiley & Sons, Inc.; 1993.

[28] Idelchik IE. Handbook of Hydraulic Resistance - Second edition, Revised and Augmented: Hemisphere Publishing Corporation; 1986.

[29] Kronwall J. Air Flows in Building Components [PhD Thesis]. Lund: Lund Institute of Technology; 1980.

[30] Eriksson D, Norberg C. Kompendium i grundläggande strömningslära (Compendium of basic fluid mechanics). Lund: Instutionen för Energivetenskaper; 2006. (in Swedish).

[31] Davidovic D, Piñon J, Burnett EFP, Srebric J. Analytical procedures for estimating airflow rates in ventilated, screened wall systems (VSWS). Building and Environment. 2012;47:126-37

[32] Nevander LE, Elmarsson B. Fukthandbok - teori och praktik (Moisture handbook - theory and practice). 2nd ed. Stockholm: AB Svensk Byggtjänst; 1994. (in Swedish).

[33] Claesson J, Nevander LE, Sandin K. Kompendium i byggnadsfysik - Värme (Compendium in building physics - Heat). Lund: Lunds Tekniska Högskola; 1984.

[34] ASHRAE. BSR/ASHRAE Standard 160P, Criteria for moisture control design analysis in buildings. Atlanta: American Society of Heating, Air-Conditioning and Refrigeration Engineers, Inc; 2009.

[35] Basset M, McNeil S. Ventilating wall cavities above windows. Journal of Building Physics. 2009;32:305-18

[36] Saelens D, Hens H. Experimental Evaluation of Airflow in Naturally Ventilated Active Envelopes. Journal of Building Physics. 2001;25:101-27

[37] Straube J, VanStraaten R, Burnett E, Schumacher C. Review of Literature and Theory. ASHRAE 1091 - Report #1. Building Engineering Group. University of Waterloo; 2004.

[38] VanStraaten R, Straube J. Field study of airflows behind brick veneers. ASHRAE 1091 - Report #6. Building Engineering group. University of Waterloo; 2004.

[39] Falk J. Ventilerad luftspalt i yttervägg - Luftomsättningar och konvektiv fukttransport (Ventilated rainscreen cladding - Air change rates and ventilation drying) [Licentiate Thesis]. Lund: Lund University; 2010. (in Swedish).

[40] Rousseau J. Drying of walls with ventilated stucco cladding: A parametric analysis. Canada Mortgage and Housing Corporation (CMHC); 1999.

[41] Ge H, Ye Y. Investigation of ventilation drying of rainscreen walls in the coastal climate of British Columbia. In: Thermal Performance of the Exterior Envelopes of Whole Buildings X. Clearwater Beach, Florida. 2007.

[42] Salonvarra M, Karagiozis AN, Pazera M, Miller W. Air Cavities Behind Claddings - What Have We Learned? In: Thermal Performance of the Exterior Envelopes of Whole Buildings X. Clearwater Beach. Florida. USA. 2007.

[43] Finch G, Straube J. Ventilated Wall Claddings: Review, Field Performance and Hygrothermal Modeling. In: Thermal Performance of the Exterior Envelopes of Whole Buildings X. Clearwater Beach. Florida. USA. 2007.

[44] Shi X, Burnett E. Ventialtion drying in enclosure walls with vinyl cladding. In: Thermal Performance of the Exterior Envelopes of Whole Buildings X. Clearwater Beach, Florida, USA. 2007.

[45] Shi X, Schumacher C, Burnett E. Ventilation drying under simulated climate conditions. ASHRAE 1091 - Report #7. The Pennsylvania Housing Research/Resource Center. The Pennsylvania State University; 2004.

[46] Lawton MD, Brown CB, Lang AM. Stucco-clad wall drying experiment. In: Thermal Performance of the Exterior Envelopes of Whole Buildings VIII. Clearwater Beach. Florida. USA .2002.

[47] Hazleden D. Envelope drying rates experiment - final report. Ottawa: Canada Mortgage and Housing Cooperation; 2001.

[48] Davidovic D, Srebric J, Burnett EFP. Modeling convective drying of ventilated wall chambers in building enclosures. International Journal of Thermal Sciences. 2006;45:180-9

[49] Schumacher C, Shi X, Burnett E. Ventilation drying in screen-type wall systems: a physical demonstration. ASHRAE 1091 - Report #3. The Pennsylvania Housing Research/Resource Center. The Pennsylvania State University; 2004.

[50] Hansen MH, Nicolajsen A, Stang B. On the influence of cavity ventilation on moisture content in timber frame walls. In: Building Physics 2002 - 6th Nordic Symposium. Trondheim, Norway. 2002.

[51] Nore K, Thue JV, Time B, Rognvik E. Ventilated wooden claddings - A field investigation. In: 7th Symposium on Building Physics in the Nordic Countries. Reykjavik. 2005.

[52] Popp W, Mayer E, Künzel H. Untersuchungen über die belüftung des luftraumes hinter vorgesetzen fassadenbekleidung aus kleinformatigen elementen. Holzkirchen: Fraunhofer Institut für Bauphysik; 1980. (in German).

[53] Sandin K. Energieffektivisering av miljonprogrammets flerbostadshus genom beständiga tilläggsisoleringssystem: Uttorkning av blöt lättbetongvägg efter utvändig tilläggsisolering med olika system. TVMB-3167. Lund: Lund Institute of Technology; 2012. (in Swedish).

[54] Straube J, van Straaten R. Field studies of ventilation drying. In: Thermal Performance of the Exterior Envelopes of Whole Buildings IX. Clearwater Beach, Florida, USA. 2004.

[55] Drumheller SC, Carll CG. Effect of cladding systems on moisture performance of wood-framed walls in a mixed-humid climate. In: Thermal Performance of the Exterior Envelopes of Whole Buildings XI. Clearwater Beach, Florida, USA. 2010.

[56] McNeil S, Bassett M. Moisture recovery rates for walls in temperate climates. In: 11th Canadian Conference on Building Science and Technology. Banff, Alberta, Canada. 2007.

[57] Hedenblad G. Materialdata för fukttransportberäkningar (Material data for moisture transport calculations). T19:1996. Stockholm: Byggforskningsrådet; 1996. (in Swedish).

[58] Hägerstedt SO, Harderup LE. Importance of a proper applied airflow in the facade air gap when moisture and temperature are calculated in wood framed walls. In: 5th International Symposium on Building and Ductwork Air-tightness. Copenhagen/Lyngby. Denmark. 2010.

[59] Hägerstedt SO, Arfvidsson J. Comparison of field measurements and calculations of relative humidity and temperature in wood framed walls. In: Thermophysics 2010 - 15th International Meeting of Thermophysical Society. Valtice. Czech Republic. 2010.

[60] Burnett E, Straube J, Karagiozis A. Synthesis report and guidelins. ASHRAE 1091 - Report #12. The Pennsylvania Housing Research/Resource Center. The Pennsylvania State University; 2004.

[61] Larsson O. Modelling of temperature profiles in a concrete slab under climatic exposure. Struct Concr. 2009;10:193-201.10.1680/stco.2009.10.4.193.

[62] Sandin K. Beständighet hos putsade fasader - probleminventering (Durability of rendered facades - inventory of problems). TVBM-3079. Lund: Lund Institute of Tehcnology; 1998. (in Swedish).

[63] Hassanzadeh M. Sprickbildning i puts på isolering - inledande laboratorieförsök och parameter studier (Cracking of render on insulation - initial laboratory investigations and parametric studies). Lund: Lund Institute of Technology; 2001. (in Swedish).

[64] Sandin K. Sprickbildning i puts på isolering - inledande studier av putsens krympning och svällning (Cracking of render on insulation - initial studies of render shrinkage and swelling). TVBM-3101. Lund: Lund Institute of Technology; 2002. (in Swedish).

[65] Sandin K. Sprickbildning i puts på isolering - inledande försök på provväggar (Cracking of render on insulation - initial tests on experimental walls). TVBM-3108. Lund: Lund Institute of Technology; 2003. (in Swedish).

[66] Hassanzadeh M. Sprickbildning i puts på isolering - undersökning av grundläggande mekanismer (Cracking of render on insulation - investigation of fundamental mechanisms). TVBM-3117. Lund: Lund Institute of Technology; 2004. (in Swedish).

[67] Sandin K. Sprickbildning i puts på isolering - försök på provväggar (Cracking of render on insulation - tests on experimental walls). TVBM-3116. Lund: Lund Institute of Technology; 2004. (in Swedish).

[68] Hassanzadeh M. Sprickbildning i puts på isolering - undersökning av grundläggande mekanismer del II (Cracking of render on insulation - investigation of fundamental mechanisms part II). TVBM-3132. Lund: Lund Institute of Technology; 2006. (in Swedish).

[69] Hassanzadeh M. Sprickbildning i puts på isolering - undersökning av grundläggande mekanismer del III (Cracking of render on insulation - investigation of fundamental mechanisms part III). TVBM-3137. Lund: Lund Institute of Technology; 2007. (in Swedish).

[70] Rodhe M. KFX03. Gothenburg: Chalmers University of Technology; 2003. p. Software for non-steady state moisture calulations.